












































# JWST observations of SN 2024abup: First Detection of CO in a broad-lined Type Ic Supernova and Constraints on r-process Nucleosynthesis

MANISHA SHRESTHA <sup>1,2</sup> LINDSEY A. KWOK <sup>3</sup> DAVID J. SAND <sup>4</sup> STAN BARTMENTLOO <sup>5</sup> COLLIN CHRISTY <sup>4</sup>  
ANDERS JERKSTRAND <sup>5</sup> K. AZALEE BOSTROEM <sup>4,\*</sup> JENNIFER E. ANDREWS <sup>6</sup> KATE D. ALEXANDER <sup>4</sup>  
YIZE DONG (董一泽) <sup>7</sup> CARL E. FIELDS <sup>4</sup> EMILY HOANG <sup>8</sup> GRIFFIN HOSSEINZADEH <sup>9</sup> BRIAN HSU <sup>4</sup>  
DARYL JANZEN <sup>10</sup> SAURABH W. JHA <sup>11</sup> JOEL JOHANSSON <sup>5</sup> JENIVEVE PEARSON <sup>4</sup> M. J. LUNDQUIST <sup>12</sup>  
DARSHANA MEHTA <sup>8</sup> AIDAN MARTAS <sup>13</sup> MARYAM MODJAZ <sup>14</sup> BERNHARD MÜLLER <sup>1</sup> CONOR L. RANSOME <sup>4</sup>  
ARAVIND P. RAVI <sup>8</sup> MATHIEU RENZO <sup>4</sup> NICOLÁS MEZA RETAMAL <sup>8</sup> BHAGYA SUBRAYAN <sup>4</sup> NATHAN SMITH <sup>4</sup>  
STEFANO VALENTI <sup>8</sup> SERGIY VASYLYEV <sup>9</sup> GIACOMO RICIGLIANO <sup>15,16</sup> PETER J. BROWN <sup>17</sup>  
MOIRA ANDREWS <sup>18,19</sup> JOSEPH FARAH <sup>18,19</sup> D. ANDREW HOWELL <sup>18,19</sup> CURTIS MCCULLY <sup>18</sup>  
MEGAN NEWSOME <sup>18,19</sup> KATHRYN WYNN <sup>18,19</sup> RYAN CHORNOCK <sup>13,20,21</sup> NATALIE LEBARON <sup>13,20,21</sup>  
RAFFAELLA MARGUTTI <sup>13,20,21</sup> MELISSA SHAHBANDEH <sup>22,23</sup> CHRIS ASHALL <sup>24</sup> AND PETER HOEFLICH <sup>25</sup>

<sup>1</sup>*School of Physics and Astronomy, Monash University, Clayton, Victoria 3800, Australia*

<sup>2</sup>*OzGrav: The ARC Centre of Excellence for Gravitational Wave Discovery, Clayton, Victoria 3800, Australia*

<sup>3</sup>*Center for Interdisciplinary Exploration and Research in Astrophysics and Department of Physics and Astronomy, Northwestern University, 1800 Sherman Avenue, 8th Floor, Evanston, IL 60201, USA*

<sup>4</sup>*Steward Observatory, University of Arizona, 933 North Cherry Avenue, Tucson, AZ 85721-0065, USA*

<sup>5</sup>*Oskar Klein Centre, Department of Astronomy, Stockholm University, Albanova University Centre, SE-106 91 Stockholm, Sweden*

<sup>6</sup>*Gemini Observatory, 670 North A'ohoku Place, Hilo, HI 96720-2700, USA*

<sup>7</sup>*Center for Astrophysics | Harvard & Smithsonian, 60 Garden Street, Cambridge, MA 02138-1516, USA*

<sup>8</sup>*Department of Physics and Astronomy, University of California, Davis, 1 Shields Avenue, Davis, CA 95616-5270, USA*

<sup>9</sup>*Department of Astronomy & Astrophysics, University of California, San Diego, 9500 Gilman Drive, MC 0424, La Jolla, CA 92093-0424, USA*

<sup>10</sup>*Department of Physics & Engineering Physics, University of Saskatchewan, 116 Science Place, Saskatoon, SK S7N 5E2, Canada*

<sup>11</sup>*Department of Physics and Astronomy, Rutgers, the State University of New Jersey, 136 Frelinghuysen Road, Piscataway, NJ 08854-8019, USA*

<sup>12</sup>*W. M. Keck Observatory, 65-1120 Māmalahoa Highway, Kamuela, HI 96743-8431, USA*

<sup>13</sup>*Department of Astronomy, University of California, Berkeley, CA 94720-3411, USA*

<sup>14</sup>*Department of Astronomy, University of Virginia, Charlottesville, VA 22904, USA*

<sup>15</sup>*Max-Planck-Institut für Kernphysik, Saupfercheckweg 1, Heidelberg D-69117, Germany*

<sup>16</sup>*Institut für Kernphysik, Technische Universität Darmstadt, Schlossgartenstr. 2, Darmstadt D-64289, Germany*

<sup>17</sup>*Department of Physics and Astronomy, Texas A&M University, 4242 TAMU, College Station, TX 77843, USA*

<sup>18</sup>*Las Cumbres Observatory, 6740 Cortona Drive, Suite 102, Goleta, CA 93117-5575, USA*

<sup>19</sup>*Department of Physics, University of California, Santa Barbara, CA 93106-9530, USA*

<sup>20</sup>*Department of Physics, University of California, 366 Physics North MC 7300, Berkeley, CA 94720, USA*

<sup>21</sup>*Berkeley Center for Multi-messenger Research on Astrophysical Transients and Outreach (Multi-RAPTOR), University of California, Berkeley, CA 94720-3411, USA*

<sup>22</sup>*Department of Physics and Astronomy, The Johns Hopkins University, 3400 North Charles Street, Baltimore, MD 21218, USA*

<sup>23</sup>*Space Telescope Science Institute, 3700 San Martin Drive, Baltimore, MD 21218-2410, USA*

<sup>24</sup>*Institute for Astronomy, University of Hawai'i, 2680 Woodlawn Drive, Honolulu, HI 96822-1839, USA*

<sup>25</sup>*Department of Physics, Florida State University, 77 Chieftan Way, Tallahassee, FL 32306-4350, USA*

## ABSTRACT

SN 2024abup is a nearby broad-lined Type Ic supernova (SN Ic-bl) in NGC 0681 at a distance of  $23.3 \pm 1.6$  Mpc. As energetic explosions of massive stars, SNe Ic-BL are considered a plausible site for rapid-neutron capture nucleosynthesis (*r*-process) and chemical enrichment from short-lived progenitors. They may also contribute to dust production in the early Universe. We present JWST near- to mid-infrared (NIR+MIR) observations (1–14  $\mu$ m) of SN Ic-bl 2024abup at +41 days after

Corresponding author: Manisha Shrestha  
manisha.shrestha@monash.edu

Email: manisha.shrestha@monash.edu

arXiv:2606.28561v1 [astro-ph.HE] 26 Jun 2026

the V band maximum (+54 days after explosion), the first-ever JWST+MIR observation of a SN Ic-bl along with radio and optical data. Using the spectral synthesis code SUMO, we identify the observed broad IR line features in SN 2024abup and find significant contributions from C, O, Mg, and carbon monoxide (CO) - the earliest detection of molecules in a core-collapse SN so far. The spectrum shows continuum emission at wavelengths greater than  $1.5 \mu\text{m}$ , which could be explained by dust—preexisting, newly formed, or a combination—heated by the SN. We do not find compelling evidence for infrared signatures of  $r$ -process elements, though our search is hampered by the presence of many broad and blended features from the non- $r$ -process elements. These new observations indicate that SNe Ic-BL could be a contributor to early-universe dust production, and suggest that if  $r$ -process elements are produced, revealing their presence from spectra requires very high-quality data and models to disentangle blends.

*Keywords:* Core-collapse supernovae(304), Type Ic supernovae(1730),  $r$ -process(1324), Dust formation(2269)

## 1. INTRODUCTION

The explosion of massive stars with  $M_{\text{ZAMS}} \gtrsim 8 M_{\odot}$  are known as core-collapse supernovae (CCSNe). Among the zoo of CCSN types, only  $\sim 1\%$  (W. Li et al. 2011; I. Shivvers et al. 2017) do not exhibit any hydrogen (H) or helium (He) and exhibit broad features, classifying them as Type Ic broad-lined supernovae (SN Ic-bl)(also see reviews by e.g. S. E. Woosley & J. S. Bloom 2006; Z. Cano et al. 2017; M. Modjaz et al. 2019). These explosions are characterized by ejecta velocities of  $20\text{--}30,000 \text{ km s}^{-1}$  (e.g. M. Modjaz et al. 2016), well above the typical  $\sim 10,000 \text{ km s}^{-1}$  for normal core-collapse SNe, along with inferred kinetic energies an order of magnitude higher. SN Ic-bl are the only type of SN that has been associated with normal long-duration gamma-ray bursts (LGRBs), however, not all SN Ic-bl are associated with LGRBs (e.g. A. Corsi et al. 2016; M. Modjaz et al. 2016; J. Japelj et al. 2018; F. Taddia et al. 2019; A. Corsi et al. 2023; G. P. Srinivasaragavan et al. 2024; G. Schroeder et al. 2025). Several competing progenitor scenarios for SN Ic-bl have been proposed to explain the stripping of H and He from the envelope: 1) mass loss via binary interaction in massive stars (e.g. P. Podsiadlowski et al. 1993; K. I. Nomoto et al. 1995), 2) mass loss via strong stellar winds of single Wolf-Rayet stars (e.g. C. M. Gaskell et al. 1986; S. J. Smartt 2009), 3) eruptions that create dense shells (P. Salas et al. 2013; T.-W. Chen et al. 2026), and 4) chemical homogeneous evolution (M. Nicholl et al. 2017; M. Renzo et al. 2026). In either case, the progenitor is expected to be a rapidly rotating massive star whose core collapse drives a hyperenergetic explosion.

The first electromagnetic counterpart to a gravitational wave (GW) source was detected for GW170817 (e.g. K. D. Alexander et al. 2017; I. Andreoni et al. 2017; I. Arcavi et al. 2017; S. Covino et al. 2017; P. S. Cowperthwaite et al. 2017; M. R. Drout et al. 2017; P. A. Evans et al. 2017; A. Goldstein et al. 2017; D. Haggard et al. 2017; M. M. Kasliwal et al. 2017; R. Margutti et al. 2017; E. Pian et al. 2017; V. Savchenko et al. 2017; S. J. Smartt et al. 2017; M. Soares-Santos et al. 2017; N. R. Tanvir et al. 2017; E. Troja et al. 2017; Y. Utsumi et al. 2017; S. Valenti et al. 2017), in the form of short-duration GRB 170817A (A. Goldstein et al. 2017; V. Savchenko et al. 2017) and subsequent kilonova emission in the form of AT 2017gfo (D. A. Coulter et al. 2017). This discovery provided a breakthrough in our search for astrophysical mechanisms to produce  $r$ -process elements (see R. Margutti & R. Chornock 2021 for a review). While the production of such material in binary neutron star mergers is confirmed, there is emerging evidence that they are not the sole source of the  $r$ -process elements. For instance, chemical abundance patterns in Milky Way halo stars and dwarf galaxies both argue for a prompt enrichment channel in the early universe, and  $r$ -process events that are substantially different from that expected from binary neutron stars (e.g., A. P. Ji et al. 2016; D. Yong et al. 2021; R. P. Naidu et al. 2022). The rate of binary neutron star mergers is also highly uncertain, and recent analysis of GW data from the O4a Laser Interferometer Gravitational-Wave Observatory (LIGO), Virgo and KAGRA collaboration run finds that the rate could be two times lower than previously expected from the O2 run (The LIGO Scientific Collaboration et al. 2025, 2026). This lower rate implies that  $r$ -process abundances seen in the Universe could not be explained by only BNS mergers as thought previously (M. R. Drout et al. 2017). Thus, another

\* LSSTC Catalyst Fellow

channel of  $r$ -process element production is likely needed to match the observed abundances (see examples, O. Pappas et al. 2015; R. P. Naidu et al. 2022; D. M. Siegel et al. 2022; A. Grichener 2025; A. Patel et al. 2025).

SNe Ic-BL have been proposed as one of the many viable mechanisms for producing heavy elements via  $r$ -process. Here,  $r$ -process material is most likely produced in stars that collapse to a black hole with an accretion disk (collapsar) but could also occur when the collapse produces a rapidly spinning, strongly magnetized neutron star (A. I. MacFadyen & S. E. Woosley 1999; D. M. Siegel et al. 2019). Recent 3D relativistic MHD simulations have found that collapsars could be the production site for a large fraction of all the  $r$ -process elements in the Universe (D. M. Siegel et al. 2019). In the simulations by D. M. Siegel et al. (2019), they found that the production of  $r$ -process elements impacts the near-infrared (NIR) photometry and spectroscopy. J. Barnes & B. D. Metzger (2022) expanded the D. M. Siegel et al. (2019) model to include a wider parameter space to investigate the possibility of detecting  $r$ -process production in SN Ic-bl. J. Barnes & B. D. Metzger (2022) find that  $r$ -process elements produce a near-infrared excess compared to regular SN Ic-bl light-curve that can be observed even during the photospheric phase (within  $\sim 75$  days). J. Barnes & B. D. Metzger (2022) finds that  $r$ -process effects are most prominent in the NIR wavelength ranges. The strength of this signature is predicted to be more visible for typical or low-mass ejecta SN Ic-bl. Recently, G. Riciigliano et al. (2025) modeled the nebular spectrum of SNe Ic-BL using a plasma model including the heavy element line list by K. Hotokezaka et al. (2022), and found that, if SNe Ic-BL are a relevant production site for  $r$ -process elements, the latter would be likely identifiable in the spectra. In particular, the imprints from these elements would be observable between  $\sim 1$  and  $10 \mu\text{m}$ , for a few  $\times 0.1\%$  of the ejecta mass being constituted by heavy species. However, there are also several theoretical works predicting that typical collapsars do not produce significant neutron-rich ejecta, leading to  $r$ -process (e.g. S. Fujibayashi et al. 2020; D. Issa et al. 2025; O. Just et al. 2015; J. M. Miller et al. 2020). Thus, there is an open question whether collapsars could be a site for  $r$ -process element production. These theoretical works underscore the need for IR observations of SN Ic-bl to answer this question of  $r$ -process productions via this alternative channel.

S. Anand et al. (2024) performed a systematic study of 25 SNe Ic-BL following the models of J. Barnes & B. D. Metzger (2022). Their analysis shows that the light curves of their sample better match  $r$ -process-free models. Their data, however, is limited to low-cadence op-

tical and near-infrared photometry. Additionally, J. C. Rastinejad et al. (2024) analyzed four SN Ic-bl associated with LGRBs using optical-to-NIR photometric data from the Hubble Space Telescope (HST) and found no conclusive evidence for  $r$ -process elements. The four SNe Ic-BL have limited NIR data at different epochs. In addition, neither of these two studies utilizes spectroscopic analysis. Thus, it is still essential to search for  $r$ -process signatures in spectroscopic data, which may be able to distinguish subtle features that broadband photometry cannot.

In addition to heavy element production, SN Ic-bl could produce dust. A significant amount of dust has been observed in high-redshift galaxies (from  $z \simeq 4$  to  $z \simeq 8$ ) (e.g., N. Laporte et al. 2017). These galaxies are too young for low-mass stars to evolve to the asymptotic giant branch (AGB) phase and produce dust (which is the major dust producer in our current universe; e.g. R. Gehrz 1989; F. Dell’Aglia et al. 2018; P. Ventura et al. 2014). Hence, other channels such as CCSNe have been proposed as a prompt channel for dust production (e.g., I. Cherchneff et al. 2026; E. Dwek & I. Cherchneff 2011; S. Liljegren et al. 2020; R. Schneider & R. Maiolino 2024). There have been several detections of CO in SN Ic, where CO can efficiently cool SN ejecta for dust formation to take place (J. Rho et al. 2021; A. P. Ravi et al. 2023; S. Tinyanont et al. 2026). These detections indicate that SN Ic could be contributing to the dust budget of the early universe; however, so far, we have not detected any CO in SN Ic-bl.

The discovery of the nearby Type Ic-BL SN 2024abup provides a great opportunity to test whether these explosions can produce  $r$ -process elements and dust. SN 2024abup was discovered on 2024-11-22 08:25:17.760 UT (60636.35 MJD) by the Asteroid Terrestrial-Impact Last Alert System (ATLAS; J. L. Tonry 2011; J. L. Tonry et al. 2018; K. W. Smith et al. 2020; M. D. Fulton et al. 2023) in NGC 0681 at a distance of  $23.3 \pm 1.6$  Mpc using the Hubble flow distance method assuming  $H_0 = 73 \pm 5$  km/sec/Mpc<sup>26</sup> (see Figure 1). It was classified as a stripped-envelope SN (C. Balcon 2024) and later confirmed as an SN Ic-bl (C. Lidman et al. 2024) (see Figure 2). We present further explosion properties such as ejecta mass, expansion velocities, nickel mass, etc., of SN 2024abup in Table 1.

In Section 2 we detail the data reduction of our photometric and spectroscopic data, and in Section 3 we analyze the properties of the host galaxy and calculate the line-of-sight extinction. We present explosion prop-

<sup>26</sup> <https://ned.ipac.caltech.edu>

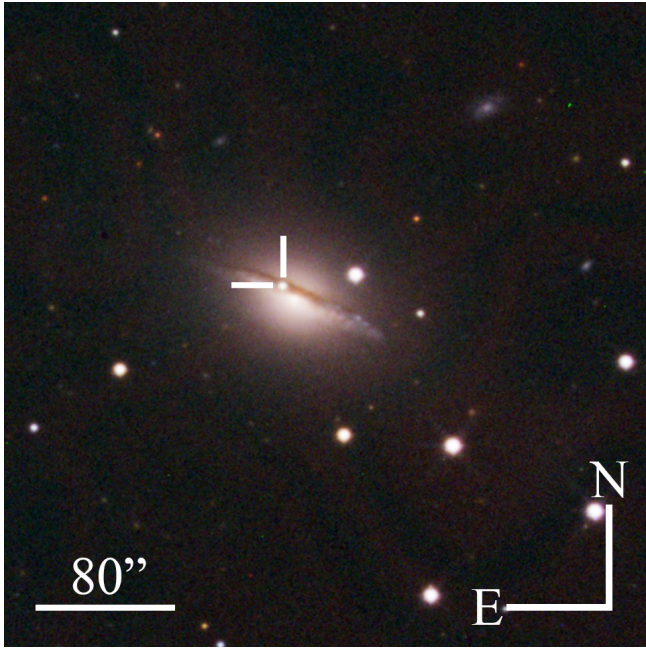


**Figure 1.** SN 2024abup in NGC 0681 taken 25 days post explosion. The image is a composite of  $g$ ,  $r$ , and  $i$  filter data from the Las Cumbres Observatory.

erties in Section 4. We present our spectral analysis in Section 5, including line identifications, model comparison, CO detection, comparison to other objects, and our search for r-process lines. The results from radio observations are presented in Section 6. Finally, we discuss our results and summarize our conclusions in Section 7.

## 2. OBSERVATIONS & DATA REDUCTION

We performed multi-wavelength photometric and spectroscopic follow-up of SN 2024abup as described below. In this work, we focus on the analysis of the optical to MIR spectrum at 41 days post maximum; detailed analysis of the additional data will be presented in future work.

### 2.1. Spectroscopy

We obtained optical, NIR, and MIR spectra of SN 2024abup with JWST and the Las Cumbres Observatory (LCO). An optical spectrum near the peak (60649 MJD) in V band and one contemporaneous to JWST observation at +41 days post V band maximum was obtained with the FLOYDS spectrographs (T. M. Brown et al. 2013) on the LCO’s 2m Faulkes Telescopes North and South (FTN/FTS) as part of the Global Supernova Project. This spectrum was reduced following standard procedures using the FLOYDS pipeline (S. Valenti et al. 2014).

We also obtained JWST NIRSpec + MIRI spectroscopy of SN 2024abup at +41 days post maximum

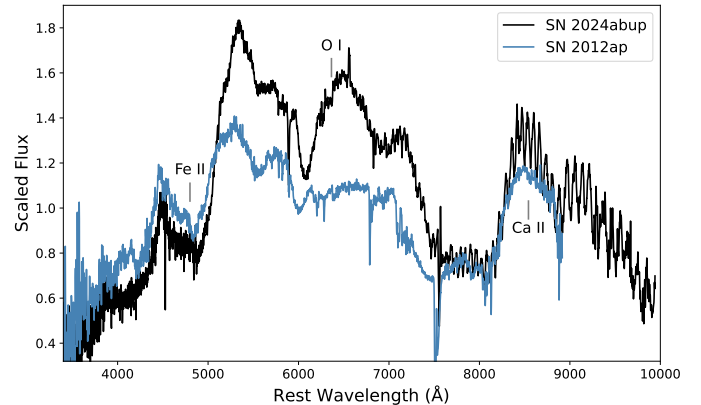


**Figure 2.** Extinction corrected optical spectrum of SN 2024abup from FLOYDS around  $V_{\max}$  on 60649.40 MJD compared to SN 2012ap, the best fit SN Ic-bl (D. Milisavljevic et al. 2015) according to SNID-SAGE (F. Stoppa & S. J. Smartt 2026), near peak in V band. The similarity between the two objects provides confirmation of SN 2024abup’s classification as a SN Ic-bl (C. Balcon 2024).

through Director’s Discretionary program JWST-DD-6803<sup>27</sup> (M. Shrestha et al. 2024) on 2025-01-15 UT. Combining the JWST data with our contemporaneous FLOYDS spectrum observed on 2025-01-09 UT, Figure 3 shows the resulting panchromatic spectrum spanning 0.4–13.5  $\mu\text{m}$ . The NIRSpec observations used the Fixed Slit (FS) medium resolution ( $R \sim 1000$ ) G140M, G235M, and G395M gratings with the F100LP, F170LP, and F290LP filters, respectively, for continuous coverage from 1–5  $\mu\text{m}$ . The MIRI observations used the Low Resolution Spectrograph (LRS;  $R \sim 100$ ), covering  $\sim 5$ –14  $\mu\text{m}$ . The total NIRSpec science exposure time, split evenly between the three gratings, was 657 s (11 min) each, and the total MIRI/LRS science exposure time was 1112 s (18.5 min).

SN 2024abup is located in a thick dust lane of its host galaxy, and we find that the stage3 MIRI/LRS spectral reductions available on MAST, produced through the automatic JWST pipeline, do not properly account for nearby host galaxy flux. The standard background subtraction is done by subtracting the two along-slit-nod dithers and then co-adding along the source trace; however, in this case, directly co-adding the nod-subtracted images results in oversubtraction in regions on either side of the source. Inspecting the stage2 two-dimensional (2D) individual nod images—after the nods have been subtracted, but prior to co-adding—we find a nearby, faint, extended trace that we identify as the host

<sup>27</sup> All JWST data is publicly available on MAST at DOI: [10.17909/0shq-ex65](https://doi.org/10.17909/0shq-ex65)

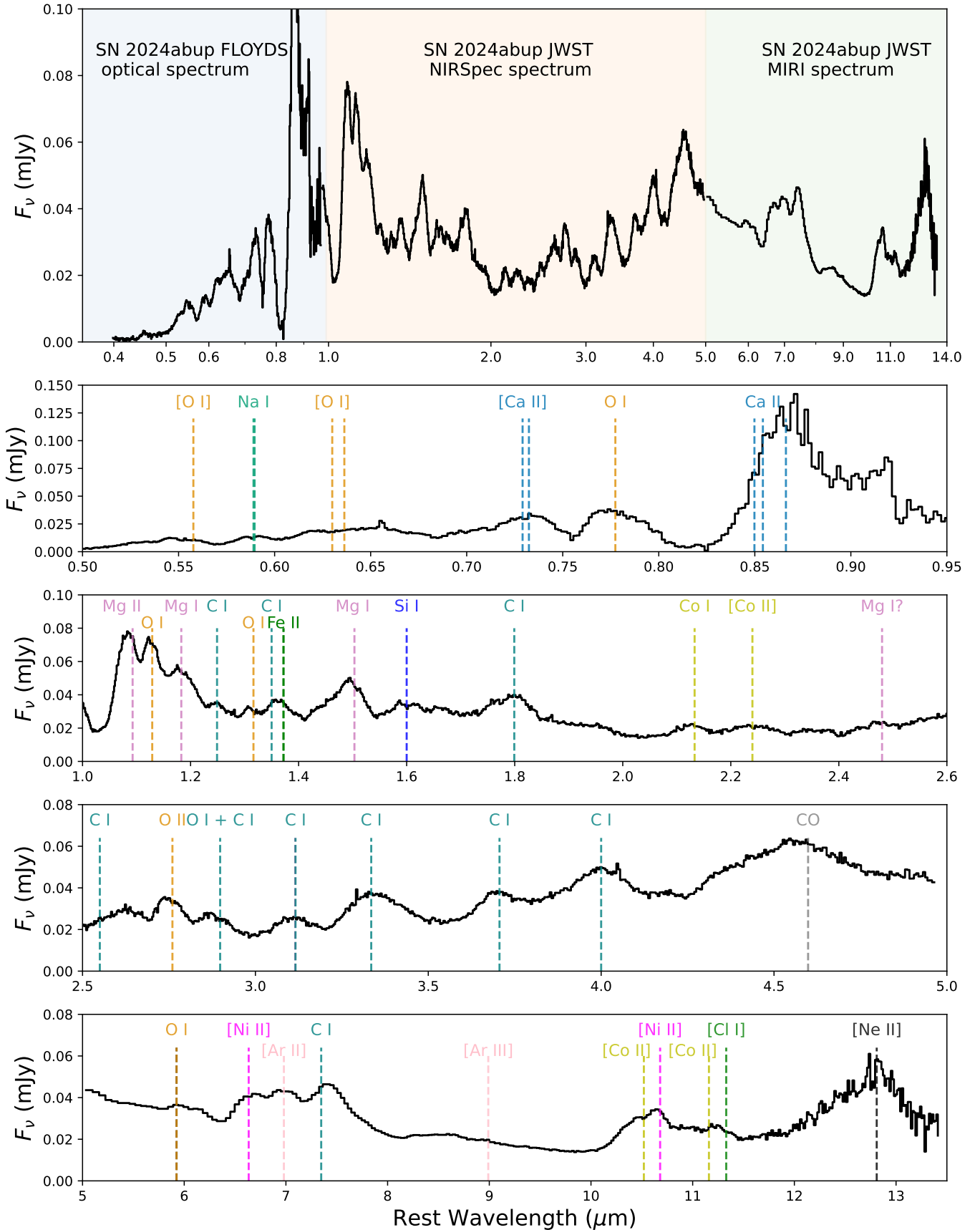


**Figure 3.** SN 2024abup spectrum spanning optical (FLOYDS) to MIR (JWST) + 41 days after the V band maximum. The top panel covers 0.4 to 14  $\mu$  m and subsequent panels zoom in on the optical spectrum, the third covers 1 to 2.6  $\mu$  m, the fourth is for 2.5 to 5  $\mu$  m, and the last one covers 5 to 14  $\mu$  m. All the major lines identified using the SUMO model (see Section 5.1 and Figure 6) are marked with dashed vertical lines.

galaxy. Extracting along this faint trace reveals that the host galaxy spectrum is dominated by emission lines from polycyclic aromatic hydrocarbons (PAHs) (see Section 5.3), consistent with expectations for an underlying dust lane.

Starting from the `stage2` products for each individual nod, we manually reextract the one-dimensional (1D) source spectrum using the JWST pipeline `extract1d` command with custom background and aperture regions chosen to avoid the host galaxy and more cleanly extract the supernova only, following methods from the public MIRI/LRS spectral extraction notebook by S. Kendrew and I. Wang.<sup>28</sup> Both individually extracted nod spectra agree within a few percent of each other, and we average them to produce the final spectrum. In the NIR, the SN trace strongly dominates over the background regions, and the spacing of the three dithered spectra makes it difficult to define a separate, uncontaminated background region, so we use the automatic JWST pipeline `stage3` product for the NIRSpec observations.

### 2.1.1. Photometry

High-cadence multi-wavelength observations were taken as part of the Global Supernova project with the Las Cumbres Observatory telescope network of 0.4 m and 1.0 m telescopes (T. M. Brown et al. 2013) in the  $B$ ,  $V$ ,  $g$ ,  $r$ , and  $i$  bands. The PyRAF-based photometric reduction pipeline was used to reduce the images as described by S. Valenti et al. (2016). We calibrate apparent magnitudes using the APASS catalog for  $g$ ,  $r$ , and  $i$  and using Landolt standard fields observed with the same telescope on the same night for  $B$  and  $V$ .

We also obtained ultraviolet images with the Ultraviolet/Optical Telescope (UVOT; P. W. A. Roming et al. 2005) on the Neil Gehrels *Swift* Observatory (N. Gehrels et al. 2004) until the SN was no longer detectable. These images were reduced using the High-Energy Astrophysics software (HEASoft<sup>29</sup>). We centered at the position of the SN with an aperture size of  $3''$ , and the background is measured from a region without contamination from other stars with an aperture size of  $5''$ . Zero points for photometry were chosen from A. A. Breeveld et al. (2010) with time-dependent sensitivity corrections updated in 2020. In the current work, we use this multiwavelength data to calculate the explosion properties, and we present the data in Figure 4.

<sup>28</sup> [https://github.com/spacetelescope/jdat\\_notebooks/blob/main/notebooks/MIRI/MIRI\\_LRS\\_spectral\\_extraction/miri\\_lrs\\_advanced\\_extraction.ipynb](https://github.com/spacetelescope/jdat_notebooks/blob/main/notebooks/MIRI/MIRI_LRS_spectral_extraction/miri_lrs_advanced_extraction.ipynb)

<sup>29</sup> <https://heasarc.gsfc.nasa.gov/docs/software/heasoft/>

**Table 1.** Properties of SN 2024abup

Parameter	Value
R.A. (J2000)	01:49:11.31
Dec. (J2000)	−10:25:27.4
Last Nondetection (MJD)	60635.16
First Detection (MJD)	60636.35
Explosion Epoch (MJD) <sup>a</sup>	60635.75
Time of $V_{\max}$ (MJD)	60649.40
Peak Absolute Magnitude ( $V_{\max}$ )	−18.75 mag
Redshift ( $z$ ) <sup>b</sup>	0.00582
Distance <sup>c</sup>	$23.3 \pm 1.6$ Mpc
Distance modulus ( $\mu$ ) <sup>c</sup>	$31.84 \pm 0.15$ mag
$E(B - V)_{\text{MW}}$ <sup>b</sup>	$0.0296 \pm 0.0344$ mag
$E(B - V)_{\text{host}}$ <sup>c</sup>	$0.79 \pm 0.06$ mag
Expansion velocity <sup>d</sup>	$18200 \pm 3200$ km/s
$M_{Ni}$	$0.24 \pm 0.01 M_{\odot}$
$M_{ej}$	$3.53 \pm 0.15 M_{\odot}$
$E_K$	$8.9 \pm 3.1 \times 10^{51}$ erg

<sup>a</sup>mid point of last nondetection and first detection

<sup>b</sup>from E. F. Schlafly & D. P. Finkbeiner (2011) from <https://irsa.ipac.caltech.edu/applications/DUST/>

<sup>c</sup>from the Na I D lines of the host galaxy and A. J. Gordon et al. (2024)

<sup>d</sup>at V band maximum

### 2.2. Radio observations

We acquired radio observations of SN 2024abup on 2025 Feb 14 (84 days after explosion) and 2025 Jun 21 (211 days after the explosion) with the Karl G. Jansky Very Large Array (VLA) under the program 24B-533 (PI: Christy). The data were taken during the A→D and C configurations, respectively, using the L, S, C, X receiver bands. We used 3C147 as the bandpass and flux-density calibrator, and J0204-1701 as the complex gain calibrator for all frequencies. The data were processed in the Common Astronomy Software Application (CASA; J. P. McMullin et al. 2007; CASA Team et al. 2022) following standard reduction procedures. We imaged the data with the CASA task `tclean`, and derived flux densities and their uncertainties using `imgfit`, by fitting an elliptical Gaussian fixed to the size of the synthesized beam at the phase center of each image.

## 3. HOST GALAXY & EXTINCTION

We examine the properties of the host galaxy of SN 2024abup. V. Kalinova et al. (2021) estimated the stellar mass ( $M_*$ ), and star formation rate (SFR) of 238 galaxies—including NGC 0681, the host galaxy of SN 2024abup—assuming a Chabrier initial mass func-

tion (IMF) (G. Chabrier 2003). We adopt their values for NGC 0681 of  $\log(\frac{\text{SFR}}{M_{\odot}\text{yr}^{-1}}) = -0.245$  and  $\log(\frac{M_{*}}{M_{\odot}}) = 10.16$ . Comparing to the SN Ic-bl host galaxy sample of M. Modjaz et al. (2020); J. Japelj et al. (2018), which spans a median mass of  $\log(\frac{M_{*}}{M_{\odot}}) = 8.9$  and a maximum of  $\log(\frac{M_{*}}{M_{\odot}}) = 9.46$ , we find that NGC 0681 is relatively massive. The SFR of NGC 0681 is consistent with the general SN Ic-bl host population (M. Modjaz et al. 2020), whose median and maximum values are  $\log(\frac{\text{SFR}}{M_{\odot}\text{yr}^{-1}}) = -0.41$  and  $\log(\frac{\text{SFR}}{M_{\odot}\text{yr}^{-1}}) = 0.42$ , respectively. We use the host redshift from the literature  $z = 0.00582$  reported by A. J. Gordon et al. (2024) and velocity of  $1704 \pm 9$  km/s, and we adopt it for all the analyses presented in this paper.

### 3.1. Line-of-sight extinction

We assume the interstellar dust extinction due to Milky Way dust to be  $E(B - V)_{\text{MW}} = 0.0297 \pm 0.0019$  mag from E. F. Schlafly & D. P. Finkbeiner (2011). SN 2024abup is located on a dust lane in NGC 0681, complicating the calculation of host galaxy dust extinction. Traditionally, the equivalent width of Na I D absorption features is used to calculate the dust extinction value; however, in this case, the absorption feature is saturated, so we cannot implement this method. Hence, we follow the prescription presented by M. D. Stritzinger et al. (2018), F. Taddia et al. (2019), and M. R. Drout et al. (2011) utilizing the SN color. In short, this method compares the  $B - V$  color evolution from 0 to +20 days after the  $B$ -band peak of stripped-envelope SN with insignificant host extinction. The difference in weighted average in this time range between the two SNe is used to estimate the host extinction value. For SN 2024abup, we compared the  $B - V$  evolution with SN 2007ru, an SN Ic-bl with no host galaxy component detected (D. K. Sahu et al. 2009). From this method, we find the host dust extinction contribution to be  $E(B - V)_{\text{host}} = 0.79 \pm 0.06$  mag. We compared the  $B - V$  evolution of SN 2024abup with several other SN Ic-bl to check the validity of this method and found that they agree well. We therefore use these extinction values for our analysis. We note that, as the focus of this paper is on the infrared wavelength range, these high extinction values do not impact the analysis significantly.

## 4. EXPLOSION PROPERTIES

From the near-peak optical spectrum of SN 2024abup (Figure 2), we estimate the expansion velocity using the Fe II absorption velocity as a proxy, as described by M. Modjaz et al. (2016). We find  $v = 18200 \pm 3200$  km/s, which falls in a normal range for SN Ic-bl with no associated GRB (M. Modjaz et al. 2016).

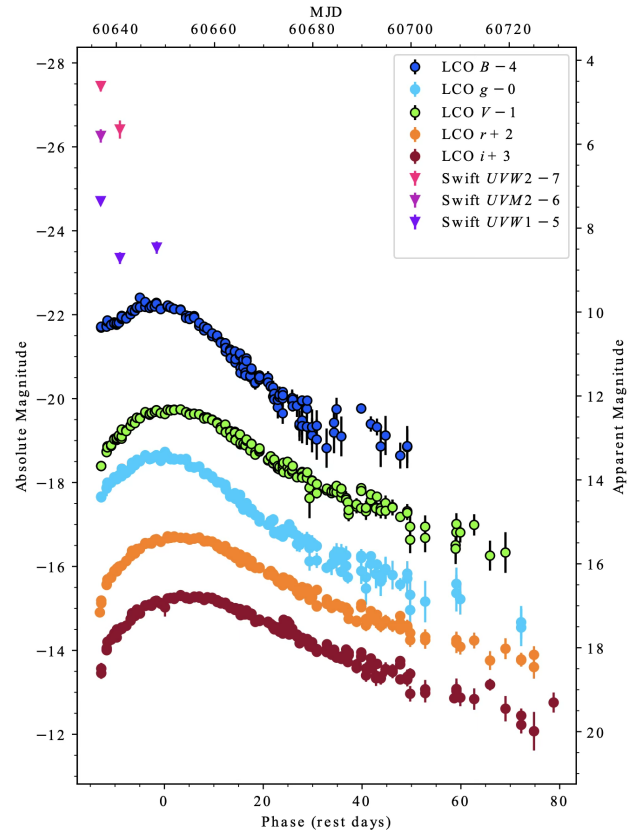


**Figure 4.** Multi-wavelength extinction corrected photometry of SN 2024abup spanning UV to optical observed using Swift and LCO. The light-curve is well sampled to 80 days after the peak in the V band.

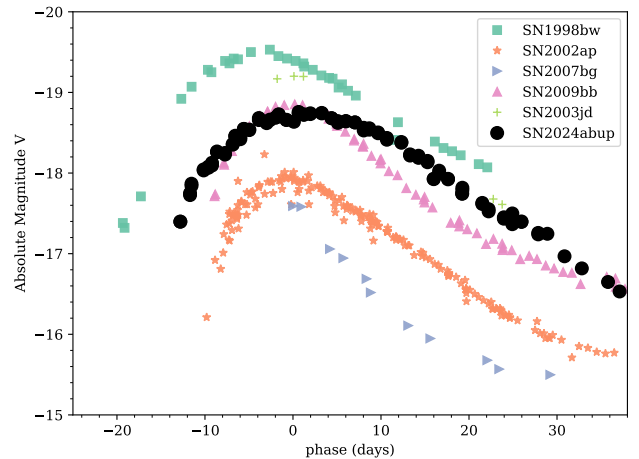


**Figure 5.** Comparison of extinction corrected absolute V band magnitudes for a few different SN Ic-bl with (SN 1998bw) and without an associated GRB. The phases are given with respect to the date of  $V_{\text{max}}$ . SN 2024abup (black circle) falls within a reasonable range with SN 1998bw, which is associated with a low-luminosity GRB, being the brightest.

We use this expansion velocity and the light curve (Figure 4) to calculate other properties of SN 2024abup, such as nickel mass ( $M_{\text{Ni}}$ ), ejecta mass ( $M_{\text{ej}}$ ), and kinetic energy ( $E_K$ ) using analytic models from W. D. Arnett (1982) and S. Valenti et al. (2008). This approach relies on some simplified assumptions, such as spherical symmetry, homologous expansion of the ejecta, a single opacity value for different compositions, and full mixing. We used the light-curve fitting package G. Hosseinzadeh et al. (2023) to generate a bolometric light curve, which is used to fit an Arnett model (W. D. Arnett 1982) using a Markov chain Monte Carlo (MCMC) method. We fit the light-curve only up to the photospheric phase ( $< 60$  days) to a one-component model as described in S. Valenti et al. (2008) where opacity  $\kappa$  is a free parameter. From this method, we obtain  $M_{\text{Ni}} = 0.2 \pm 0.1 M_{\odot}$ ,  $M_{\text{ej}} = 3.6 \pm 0.2 M_{\odot}$ ,  $\kappa = 0.02 \pm 0.01$  and  $E_K = 8.9 \pm 3.1 \times 10^{51}$  erg as presented in Table 1. The corner plot for the fit is shown in Figure A.1. Comparison of explosion properties of SN 2024abup with other SN Ic-bl presented by F. Taddia et al. (2019) shows that this transient falls in a normal range across all the properties for the SNe Ic-BL population. Additionally, the evolution of the light curve of SN 2024abup is similar to other SN Ic-bl population as show in Figure 5.

## 5. SPECTRAL ANALYSIS

We mark the dominant contributing ions/molecules to prominent spectral features in the JWST spectrum, including previously unidentified lines at  $\lambda > 2.5 \mu\text{m}$  as shown in Figure 3. Most of these line identifications are based on a SUMO NLTE spectral model (see Section 5.1 and Figure 6). As in the optical spectrum, and characteristic of the Ic-bl class as a whole, SN 2024abup also exhibits broad and blended features at these longer wavelengths that are difficult to separate cleanly.

A large fraction of previous observations of SNe Ic-bl have been limited to optical and NIR wavelengths ( $< 2.5 \mu\text{m}$ ) at comparable epochs. M. R. Siebert et al. (2024) and J. C. Rastinejad et al. (2025) have recently presented JWST spectra of two SNe Ic-bl spanning 1 to  $5 \mu\text{m}$ ; however, the spectrum of SN 2025kg was obtained near peak brightness, and that of SN 2023adta suffers from low signal-to-noise. Here we present a spectrum of SN 2024abup spanning 0.4–14 micron (Figure 3), and we employ the spectral modeling described below to aid in identifying the MIR features.

### 5.1. Spectral Modeling with SUMO

We compare the JWST NIRSpec and MIRI spectra to a model created using the SUMO spectral synthesis code (A. Jerkstrand et al. 2011, 2012) in order to identify the

contribution of different ions in the production of spectral features and to constrain potential  $r$ -process signatures. SUMO is a Monte Carlo radiative transfer code that takes as input an ejecta model of the exploded star and then solves the non-local thermodynamic equilibrium (NLTE) equations for the temperature, excitation, and ionization structure in the SN ejecta. We summarize our spectral modeling setup below, and give a detailed description in Appendix D.

To model the +41-day spectrum of SN 2024abup, we use a massive star model with  $M_{\text{He},i} = 12.0 M_{\odot}$  ( $M_{\text{ej}}$ ) evolved until core collapse by S. E. Woosley (2019), and exploded by T. Ertl et al. (2020). After prompt removal of the hydrogen envelope (mimicking Roche-lobe overflow to a binary companion but see (E. Laplace et al. 2021)), this star lost its entire helium envelope effectively due to stellar winds. This is one of the reasons for choosing this particular model; lower-mass models retained some of their helium envelope until explosion, resembling Type Ib SNe rather than Type Ic SNe. Another reason is the model’s large expansion velocities ( $v \sim 8500 \text{ km s}^{-1}$ ), leading to a better match to a Type Ic/Ic-bl than its lower-mass counterparts. The main ejecta properties of this model are summarized in Table 4. As this ejecta model contains no  $r$ -process elements, it enables a search for  $r$ -process signatures in SN 2024abup; when a feature present in SN 2024abup is not present in the model spectrum, and this feature matches an  $r$ -process transition, it would then be a good candidate for an  $r$ -process signature.

In Figure 6, we show the SUMO model spectrum compared to the observations, with the dominant ion contributions in the model marked. While the strengths of the model lines do not match the observed spectrum for every feature, the model successfully reproduces most of the spectral features seen in SN 2024abup, providing reliable line identifications. We note that no extensive grid of model comparisons or parameter fine-tuning was performed to try to match the SN 2024abup spectrum perfectly; our interest here is primarily one of line identification. A more extensive modeling effort is deferred to a future article (Barmantloo et al., in prep.).

### 5.2. $r$ -process elements

To identify possible  $r$ -process lines in the SN 2024abup spectrum, we use a line list generated by G. Ricigliano et al. (2025). All the lines from G. Ricigliano et al. (2025) are plotted along with the SN 2024abup spectrum Figure B.1. We note that G. Ricigliano et al. (2025) computed these lines for the nebular phase of SN Ic-bl; however, the JWST spectrum of SN 2024abup

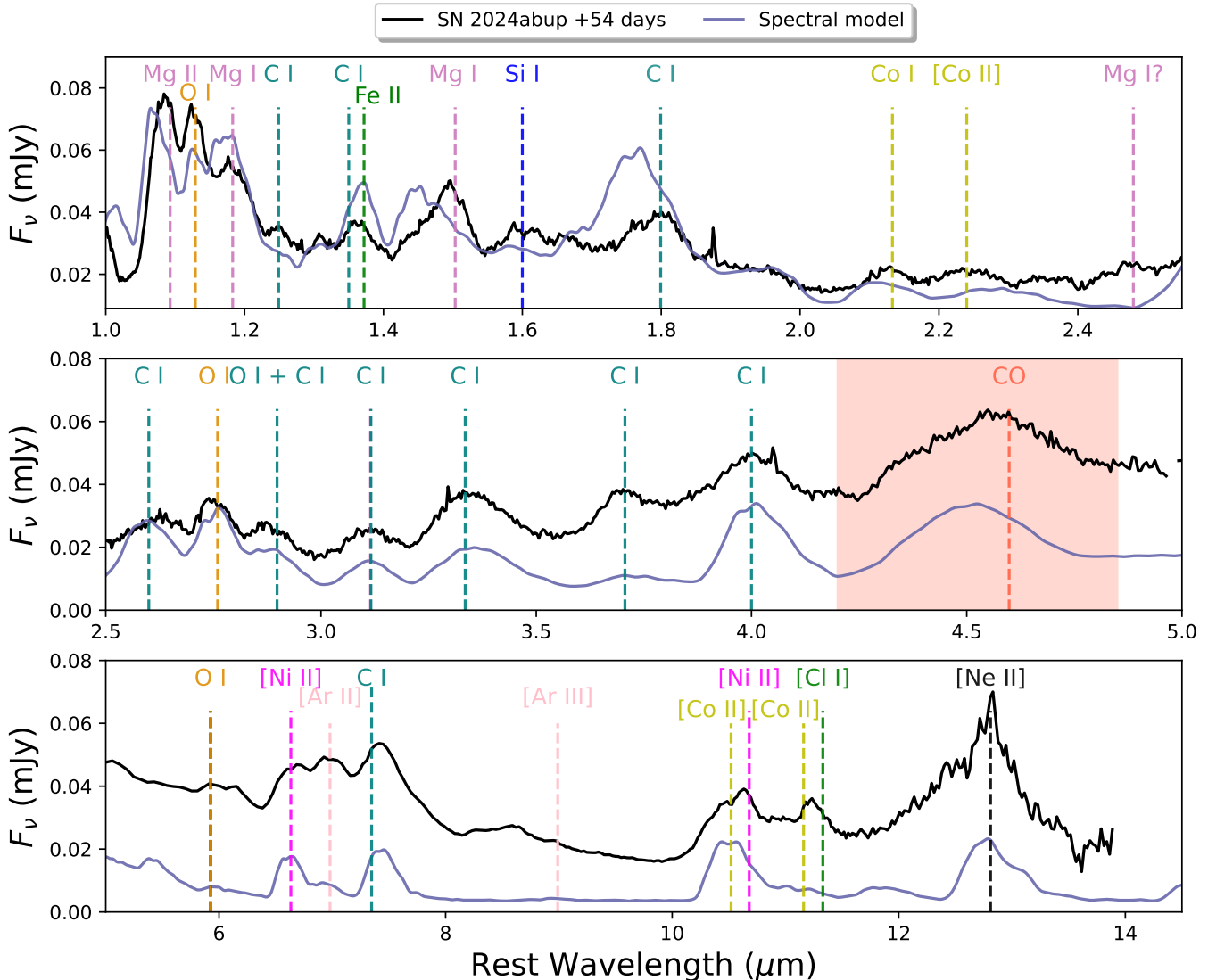


**Figure 6.** SN 2024abup compared to model from SUMO. The model is able to reproduce several observed spectral features. However, there are differences in the strength, which is expected as this model is not fine-tuned for this particular case. Overall, the observed continuum is higher than the model for wavelengths greater than  $\sim 3 \mu\text{m}$ , which could be due to the presence of dust in the SN or the host galaxy or both, which is not included in the model. The shaded region in red shows the CO feature predicted by the model and the observed spectral feature in the same wavelength regime.

is not fully nebular because we still observe absorption features.

We find several potential matches for lines predicted by G. Ricigliano et al. (2025) for SN Ic-bl in the case with original and boosted ionization rate of heavy elements that align with spectral features in the spectrum, shown in Figure 7. We find that [Rb III] ( $\lambda 1.35 \mu\text{m}$ ), [Pd III] ( $\lambda 3.09 \mu\text{m}$ ), [Br IV] ( $\lambda 3.34 \mu\text{m}$ ), [Se III] ( $\lambda 4.55 \mu\text{m}$ ) and [Sn I] ( $\lambda 5.91 \mu\text{m}$ ) align with prominent features we see in the spectra. Out of these lines, only [Sn I] could be produced without artificially boosting the ionization of these elements. For all of these features, we find that alternatively they could be attributed to non- $r$ -process

elements as we illustrate in Figure 7. SUMO can reproduce these features without  $r$ -process ions in the code. Though, the strength and the shape of these features do not match accurately, these lines are more likely to be produced by non- $r$ -process elements. Nevertheless, we cannot rule out the possibility that contributions from  $r$ -process elements are blended with those of other ions present in the SUMO model.

We further investigate possible  $r$ -process element signatures in SN 2024abup in the following sections. In Section 5.2.1 we calculate the  $r$ -process ionic mass production in the limit that the features in SN 2024abup, which aligned with predictions, are produced entirely

by heavy elements. Next, in [Section 5.2.2](#), we compare the NIR spectrum of SN 2024abup with observations of transients that have been proposed to possess  $r$ -process signatures.

### 5.2.1. Ionic mass limits

At the relatively early epoch of +41d, the IR lines arising from low-level intra-multiplet transitions can be expected to be formed in LTE (see e.g. [Barmantloo & Jerkstrand 2026](#), submitted). If the line is optically thin, the luminosity is then

$$L = M_{\text{ion}} (\mu m_p)^{-1} A h\nu \frac{g_u}{Z(T)} e^{-E_u/kT}. \quad (1)$$

Here,  $\mu$  is the atomic weight of the ion,  $A$  is the Einstein coefficient for spontaneous emission,  $g_u$  is the statistical weight of the line's upper level,  $E_u$  its energy and  $Z(T)$  is the partition function ([A. Jerkstrand 2017](#)). The exponential factor will likely be close to unity at these epochs in the MIR ( $\gtrsim 3 \mu\text{m}$ ) as the ejecta are still quite hot ( $kT \gtrsim hc/(3 \mu\text{m})$  for  $T > 5000$  K). Then, rearranging in terms of typical values,

$$L \approx 10^{39} \left( \frac{M_{\text{ion}}}{10^{-4} M_{\odot}} \right) \left( \frac{\mu}{80} \right)^{-1} \frac{g_u}{Z(T)} \times \left( \frac{\lambda}{3 \mu\text{m}} \right)^{-1} \times A \text{ erg s}^{-1}. \quad (2)$$

The characteristic line luminosity of the features measured in the observed spectrum is a few times  $10^{39}$  erg  $\text{s}^{-1}$ , which is consistent with optically thin LTE emission from  $\mathcal{O}(10^{-4}) M_{\odot}$  of the corresponding ion if the Einstein coefficient for spontaneous emission (the A-value) is of order unity. In [Table 2](#) we give the specific corresponding ionic masses if the luminosity in a feature is assumed to come from this element, and the line is formed under LTE, optically thin conditions. Here, the specific line luminosity measurements were done by integrating flux over the wavelength for the lines with respect to the continuum and converting the flux to luminosity using the distance of SN 2024abup.

For a line to be optically thin, the Sobolev optical depth ([V. V. Sobolev 1957](#)), given by (assuming most ions are in the ground state)

$$\tau_S = 0.4 \times A \times \left( \frac{\lambda}{3 \mu\text{m}} \right)^3 \times \left( \frac{M_{\text{ion}}}{10^{-4} M_{\odot}} \right) \left( \frac{\mu}{80} \right)^{-1} \times \left( \frac{v_{\text{exp}}}{8000 \text{ km s}^{-1}} \right)^{-3} \left( \frac{f}{0.1} \right)^{-1} \frac{g_u}{g_l} \left( \frac{t}{50 \text{ d}} \right)^{-2}, \quad (3)$$

should be  $< 1$ . Here,  $f$  is the filling factor (fraction of volume occupied by material containing the element).

Thus, for IR lines with  $A \approx 1 \text{ s}^{-1}$ , 41 d after the V band maximum can be a typical time at which transition to optical thinness occurs ( $\tau_S$  becomes  $< 1$ ). If it has not occurred, we would expect the line to form more of a P-Cygni like feature than a pure emission feature, and higher mass solutions can be allowed compared to the optically thin case.

The solar abundance mass ratio of e.g., Se/Fe is around  $10^{-4}$ . If we take  $0.1 M_{\odot}$  as the characteristic iron production, an average SN would then need to make  $\sim 10^{-5} M_{\odot}$  of Se to generate the solar abundance (the contribution by Type Ia SNe to the iron production, and the s-process to the Se production, are both roughly 50% so they roughly cancel out). If only SN Ic-bl produce the Se, then Se/Fe ratio increases to  $\sim 10^{-3} M_{\odot}$  as these are about a factor 100 rarer. These estimates, combined with the ionic mass limits derived in [Table 2](#), show that the JWST observations are sensitive enough to make meaningful tests of  $r$ -process production. A model or assumption is still needed about the ionization state of the  $r$ -process material. Neutral, singly and doubly ionized states are most common in SNe at these phases, so the [Sn I], [Pd III], and [Se III] limits are likely more constraining than the [Br IV] one.

Ultimately, we cannot put clear upper limits on Pd, Br, Se content in the ejecta of SN 2024abup, because the epoch of our JWST spectrum is such that the ejecta may still be optically thick in the candidate lines. Observations at somewhat later epochs would alleviate this issue. For Sn, however, if a mass more than  $5 \times 10^{-5} M_{\odot}$  were present, and to a significant extent in the neutral state, the table shows that a much stronger feature would have been observed at  $5.91 \mu\text{m}$ . With the solar Sn/Fe mass ratio at  $6 \times 10^{-6}$ , this mass limit is borderline constraining for the case of only Ic-BL SNe, making Sn (expected Sn mass then  $6 \times 10^{-5} M_{\odot}$  per event).

### 5.2.2. Comparison with other transients with $r$ -process lines

Observational signatures of  $r$ -process elements were detected in NIR spectra of AT 2017gfo ([M. M. Kasliwal et al. 2022](#)) and GRB 230307A ([A. J. Levan et al. 2024](#); [J. H. Gillanders & S. J. Smartt 2025](#)) (but see [P. Arunachalam et al. 2025](#)). In search of similar features in SN 2024abup, we compare the NIR spectrum to three different types of transients ([Figure 8](#)): 1) SN 1998bw ([F. Patat et al. 2001](#)), the well-studied, canonical SN Ic-bl associated with a low-luminosity GRB; 2) AT 2017gfo ([E. Pian et al. 2017](#)), a kilonova associated with a binary neutron star merger; and 3) GRB 230307A ([A. J. Levan et al. 2024](#)), an LGRB with kilonova-like emission. The two SN Ic-bl have similar prominent lines present. In contrast, AT 2017gfo and GRB 20230307A do not con-

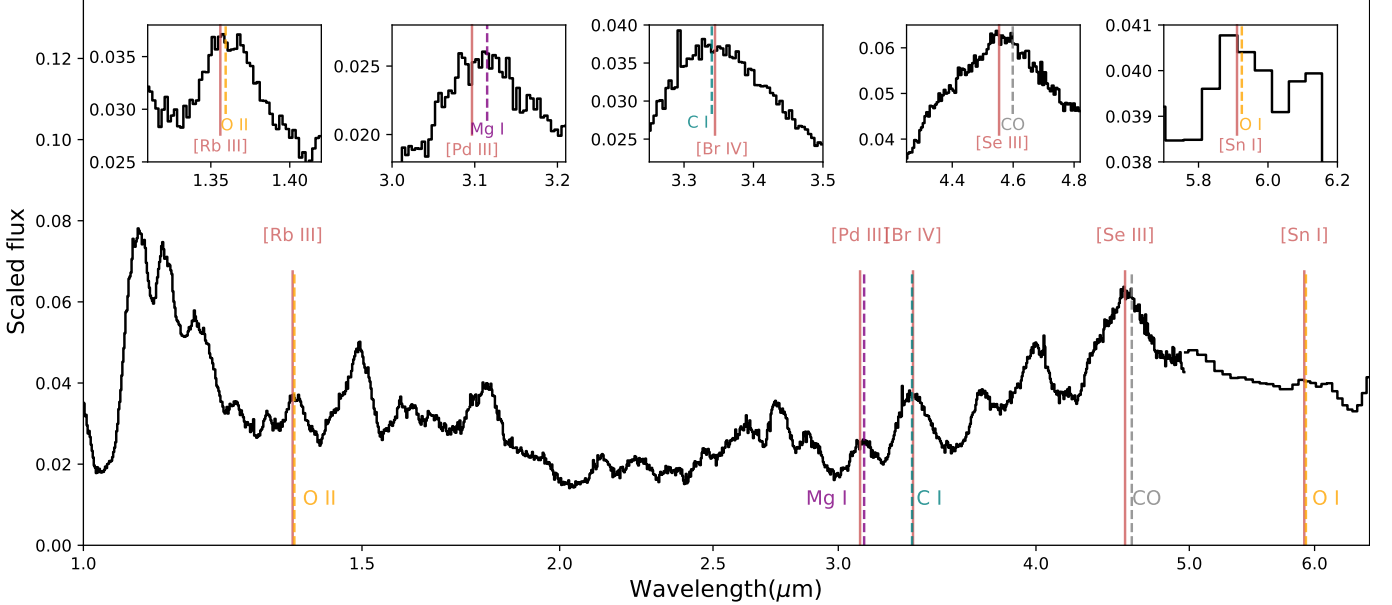


**Figure 7.** JWST spectrum of SN 2024abup at +41 days after V band maximum, overlaid with  $r$ -process element lines from G. Ricigliano et al. (2025) (solid red) and light element lines (colored dashed). The spectral features are more consistent with light elements, though line broadening may produce blending that complicates this identification. Insets show zoomed views of each individual feature.

Wavelength	Candidate	$L_{obs}$ (erg s $^{-1}$ )	A (s $^{-1}$ )	$g_u/Z(T)$	Ion mass (LTE,thin) ( $M_{\odot}$ )	$\tau_s$	Comment
3.10 $\mu m$	[Pd III]	$1 \times 10^{39}$	0.86	0.52	$\leq 4.5 \times 10^{-4}$	$\leq 0.42$	C I contam.
3.34 $\mu m$	[Br IV]	$4 \times 10^{39}$	0.33	1.45	$\leq 4.7 \times 10^{-3}$	$\leq 2.9$	C I contam.
4.55 $\mu m$	[Se III]	$5 \times 10^{39}$	0.14	1.10	$\leq 1.5 \times 10^{-2}$	$\leq 9.7$	CO contam.
5.91 $\mu m$	[Sn I]	$1 \times 10^{37}$	0.084	0.58	$\leq 4.4 \times 10^{-5}$	$\leq 0.018$	No contam.?

**Table 2.** Constraints on ionic masses under the assumption of LTE, optically thin formation, for  $T = 5000$  K. The  $\tau_s$  column shows the optical depths for the limiting masses using the Eq. 3 parameters. We limit the list to  $>3 \mu m$  lines as it's mainly these that give temperature-independent results.

tain many spectral features reminiscent of SN Ic-bl, and instead exhibit a feature at  $\sim 2.1 \mu m$  that has been interpreted as [Te III] in both (M. M. Kasliwal et al. 2017; A. J. Levan et al. 2024; J. H. Gillanders & S. J. Smartt 2025). This [Te III] feature is significantly broader and more prominent in AT2017gfo than in GRB 230307A, which might be due in part to the earlier phase.

There is also a bump in the spectrum of SN 2024abup and a broader feature in SN 1998bw (though with lower signal-to-noise) near the [Te III] line. We investigate if another line from lighter elements could be responsible for the bump in SN 2024abup and find that Mg II is a likely alternative (Figure 8). The bump is more centered on the Mg II line, and blue-shifted relative to the [Te III] line. Most of the other lines in SN 2024abup are redshifted, and other Mg I and Mg II lines are present elsewhere in the spectrum, so we attribute this feature to be Mg II, rather than [Te III]. However, we cannot rule out a weak contribution from [Te III]. Future

fully nebular phase IR spectroscopy of SN Ic-bl would strengthen constraints on the production of  $r$ -process elements in collapsars. We note that this feature could potentially account for the  $\sim 2.1 \mu m$  signal observed in GRB 230307A; however, this interpretation is unlikely, given the overall interpretation of the source being a neutron star merger (in which alpha elements are not generally synthesized).

### 5.2.3. Comparison with SN 2023dbc

Since the launch of JWST, there is a growing sample of observations of SNe at IR wavelengths. However, there are very few JWST observations of stripped envelope SN (SESN). So far, the Type Ic SN 2023dbc (M. Shahbandeh et al. 2023) is the only SESN with 1–14  $\mu m$  coverage at a similar phase as SN 2024abup. We note that SN 2023dbc has also been classified as Type Ib by M. Yamanaka et al. (2026). In either case, it is an SESN and is expected to have similar lines as SN Ic-bl; however, these features are broader and more blueshifted in SN

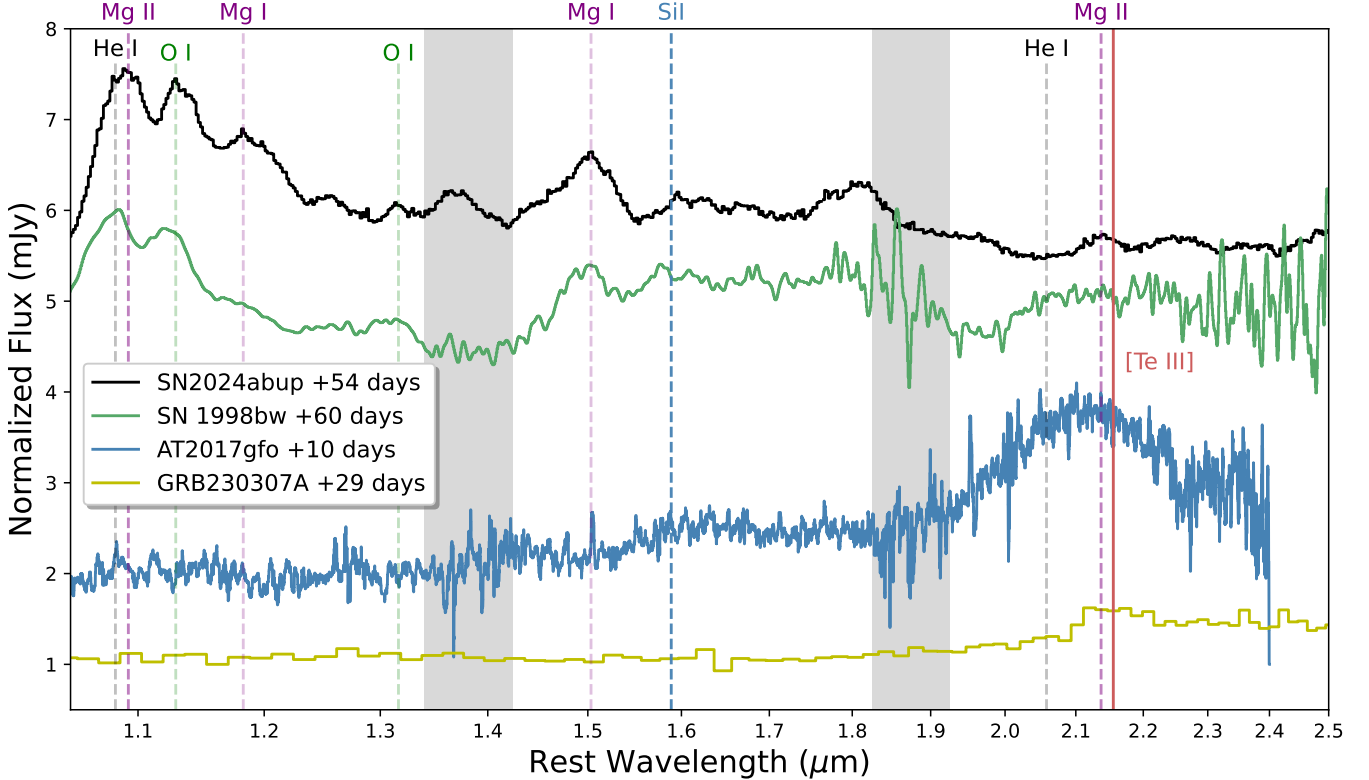


**Figure 8.** Comparison of the NIR spectrum of SN 2024abup at +41 days with SN 1998bw (F. Patat et al. 2001), AT 2017gfo (E. Pian et al. 2017), and GRB 230307A (A. J. Levan et al. 2024). Similar lines are seen for both SN 1998bw and SN 2024abup. The [Te III] line is identified in AT2017gfo and GRB230307A as a signature of  $r$ -process element production. There is a bump in SN 2024abup near the [Te III] line, but it is better explained by Mg II in this case.

Ic-bl due to the higher velocity of the ejecta, as shown by a large sample study by M. Modjaz et al. (2016). Hence, this makes comparison with SN 2023dbc an ideal case to search for  $r$ -process signatures. SN 2023dbc is located in the very nearby galaxy M108 ( $\sim 10$  Mpc). We compare the JWST spectra of SN 2023dbc (M. Shahbandeh et al. 2023) taken at +36 days since the  $r$  band maximum (we use the  $r$  band maximum to be at MJD 60030.6 from M. Yamanaka et al. 2026) with SN 2024abup at +41 days (Figure 9). The comparison of these two spectra is valuable to study the properties in the MIR wavelength regime. Additionally, we can simultaneously investigate the presence of any  $r$ -process element contribution in the SN 2023dbc spectrum that coincides with predicted features, as shown in Figure 7. Notably, for normal SNe Ic, J. Barnes & B. D. Metzger (2022) predict that hints for the presence of hypothetical  $r$ -process material would appear only for the compositional mixing in the ejecta being particularly efficient.

The spectra are overall similar between the two events, but with several key differences highlighted in Figure 9. In the MIR SN 2024abup shows stronger CO emission and a more pronounced continuum, which we associate

with dust (see Section 5.3). Another major difference is the presence of prominent He I emission lines in SN 2023dbc (shown in blue) that are not present in SN 2024abup, indicating a higher degree of envelope stripping in the progenitor of SN 2024abup. In contrast, the [Ar II] line (and to a lesser extent the weak [Ar III] line) is more pronounced in SN 2024abup. The presence of Ar lines could also indicate explosive O burning, which is expected in massive star explosions (S. E. Woosley et al. 2002).

Comparison of spectra in Figure 9 reveals that the broad features in SN 2023dbc align with those in SN 2024abup at wavelengths consistent with theoretically predicted  $r$ -process elements. The presence of these features in SN 2023dbc casts doubt on the formation of  $r$ -process elements in SN 2024abup. However, the features coincident with [Br IV] and [Se III] are more pronounced in SN 2024abup. This could potentially indicate a minor production of these heavy elements in SN 2024abup.

### 5.3. CO & Dust detection

CCSNe have been proposed as major producers of dust in high-redshift galaxies (A. Nanni et al. 2025),

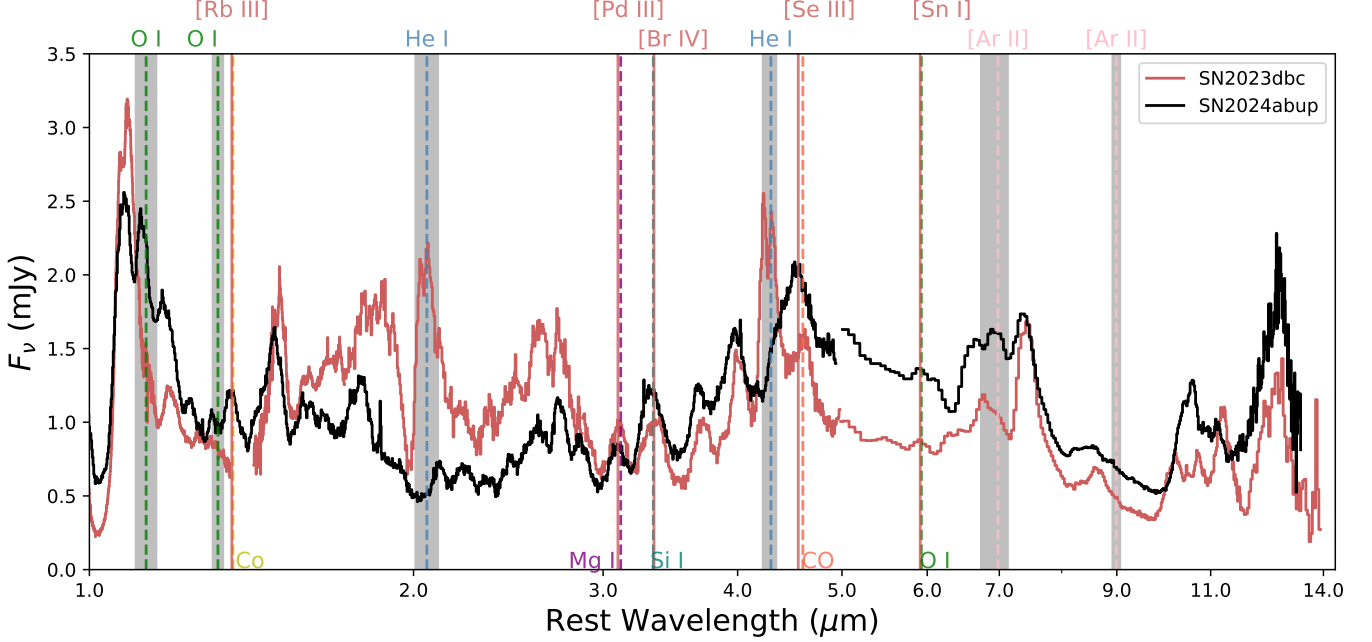


**Figure 9.** Comparison of the JWST NIR + MIR spectra of SN 2024abup (+41 days) and SN Ic 2023dbc (+36 days) (M. Shahbandeh et al. 2023). Major lines that are different between the two are shown in shaded gray regions. Lines from light and heavy species are indicated by dashed and solid lines, respectively. One of the major differences is the presence of prominent He I features in SN 2023dbc, which are absent in the case of SN 2024abup. Additionally, we detect O I lines in SN 2024abup, which are not present in SN 2023dbc. The CO feature in SN 2024abup is more prominent than in SN 2023dbc.

due to their short lifetimes and the growing evidence for dust production in nearby CCSNe (K. Medler et al. 2025; T. Mera et al. 2026). The detection of CO in SN spectra is an important precursor for dust formation, because CO plays a crucial role in cooling SN ejecta to conducive temperatures and provides a seed for condensation. While CO and dust have been detected most frequently in Type II SN (e.g., A. Sarangi et al. 2018; S. H. Park et al. 2025; K. Medler et al. 2025; T. Mera et al. 2026), dust and molecules are also expected to form in SESN (e.g., S. Liljegen et al. 2020). Observationally, CO emission was detected in a few Type Ic SN (e.g. J. Rho et al. 2021; A. P. Ravi et al. 2023; S. Tinyanont et al. 2026). However, CO or dust signatures have not previously been detected in Ic-BL.

Given the location of SN 2024abup in a dust lane of NGC 0681, the dust continuum could be attributed to host galaxy dust heated by SN 2024abup. Though we have attempted to subtract the host galaxy contribution during the data reduction, there could be some residual due to imperfect background subtraction. Alternatively (or additionally), it could be attributed to dust in the local environment produced by the previous mass loss from the progenitor or newly formed dust. The detection of CO suggests that fresh dust will form at later times; however, it is unclear how much dust may already have formed. We observe several MIR features that we

attribute partially to emission from polycyclic aromatic hydrocarbons (PAHs). Comparing with the extracted host galaxy trace, we suggest that these PAH lines predominantly arise from the underlying host galaxy (Figure 10).

The strongest CO feature observed in SN 2024abup is the broad, fundamental ro-vibrational mode around  $4.6 \mu\text{m}$ . There is a prominent, broad feature in SN 2024abup in this wavelength regime, and the SUMO model demonstrates a similar feature in the model, which is composed of CO emission as shown in Figure 6. In the model,  $1.9 \times 10^{-5} M_{\odot}$  of CO is created, so that (assuming an underlying continuum in SN 2024abup around the CO feature) SN 2024abup is estimated to have produced a similar amount of CO (see Figure 6). S. Liljegen et al. (2020) predict that molecules like CO form in SESN between 100-600 days post-explosion and that  $10^{-4} M_{\odot}$  of CO is produced by  $\sim 100$  days. SN 2024abup was observed at a somewhat earlier phase (+54 days), so that our somewhat lower estimate can be said to be on the order of what these models predict. We note that we do not observe the CO first overtone at  $\sim 2.3 \mu\text{m}$ , which is expected to be weaker in strength than the  $4.6 \mu\text{m}$  feature (J. Spyromilio et al. 1989). The SUMO model does not predict the CO feature at  $\sim 2.3 \mu\text{m}$  at this phase either.

In addition to the CO detection, SN 2024abup exhibits a continuum excess in the NIR and MIR (see Figure 10) compared to the SUMO model as well as the continuum of SN 2023dbc. Qualitatively, we fit the excess in continuum at wavelengths greater than  $1.5 \mu\text{m}$  with carbonaceous dust (pre-existing or newly formed) heated by the SN. We use the analytical work from B. S. Hensley & B. T. Draine (2023) to model the dust continuum from a combination of graphite and silicate. For this fit, we model the dust contribution such that the continuum level matches at  $\sim 10 \mu\text{m}$ . We ensured that the dust continuum did not exceed the observed spectrum at any wavelength. From this qualitative analysis, we find that silicate (graphite) dust with a mass of  $\sim 0.05 M_{\odot}$  ( $\sim 0.009 M_{\odot}$ ) of grain size  $0.1 \mu$  at a temperature of 700 K (300 K) reproduces the observed continuum the best.

## 6. JET CONSTRAINTS FROM RADIO OBSERVATIONS

All SN associated with LGRBs have been SN Ic-bl; however, most SN Ic-bl do not have an observationally associated LGRB. Prompt gamma-ray emission from LGRBs is detected only when we are located close to the initial jets' opening angle. Thus, it could be the case that all SN Ic-bl produce LGRB, but the jet is off-axis. Radio wavelengths are favored to detect off-axis jets when the SN jet has decelerated to sub-relativistic velocity. As of now, off-axis GRBs have not been discovered in this way (A. Corsi et al. 2016, 2023) except, most recently, PTF10tqv, the best off-axis SN Ic-bl candidate (G. Schroeder et al. 2025).

SN 2024abup was not associated with a LGRB, so we searched for an off-axis jet using Very Large Array (VLA) radio observations at two different epochs. We do not detect a source at the location of SN 2024abup in either epoch and report the  $3\sigma$  upper limits on the flux density in Table 3. We also show these limits in context with the broader SNe Ic-BL population in Figure 11. All SN Ic-bl radio detections have been attributed to the SN shock rather than an off-axis jet (e.g, S. R. Kulikarni et al. 1998; E. Berger et al. 2002; A. M. Soderberg et al. 2006; P. Salas et al. 2013; A. M. Soderberg et al. 2010) except for the case of PTF10tqv (G. Schroeder et al. 2025). We further compare our non-detections to VegasAfterglow (Y. Wang et al. 2026) models of a typical GRB-like relativistic jet viewed at a maximally off-axis angle ( $\theta_{\text{obs}} = 90^\circ$ ). Since more on-axis viewing angles would produce brighter radio emission at all epochs, our non-detections rule out the presence of a standard jet for a wide range of viewing angles. This suggests that any jet associated with SN 2024abup must either be intrinsically weaker than typical GRB jets or prop-

agate through a particularly low-density circumstellar environment. The absence of detectable radio emission from both an off-axis jet and the SN shock is consistent with a progenitor that lacked significant pre-explosion mass loss.

## 7. DISCUSSIONS & CONCLUSIONS

In this work, we present near and mid-IR JWST observations of the very nearby Type Ic-bl, SN 2024abup. We obtained a JWST spectrum spanning  $1\text{--}14 \mu\text{m}$  at +41 days after the maximum. The spectrum contains many broad, previously unobserved features that we identify using ion contributions from a SUMO spectral synthesis model (A. Jerkstrand et al. 2011). The IR spectrum of SN 2024abup is well modeled with a massive star model with  $M_{\text{He,i}} = 12.0 M_{\odot}$  ( $M_{\text{ej}}$ ) without any  $r$ -process elements in the ejecta. We find that most of the observed features are also present in the model without inclusion of  $r$ -process elements (T. Ertl et al. 2020), although the model does not yet match the detailed shapes and strengths of individual lines.

We find the photometric evolution of SN 2024abup to be similar to that of other SN Ic-bl. The values for various explosion properties we obtain for SN 2024abup fall in a normal range compared to a large population of SN Ic-bl. We find the host galaxy of SN 2024abup to be on the more massive side than the general SN Ic-bl population; however, the SFR of the galaxy is normal.

Additionally, we search for  $r$ -process lines in the SN 2024abup spectrum based on theoretical models by G. Ricigliano et al. (2025). We find some broad features overlapping  $r$ -process lines that are predicted by the model, as shown in Figure 7. We further constrain the  $r$ -process ionic mass in SN 2024abup by considering that the observed features are consistent with the lines predicted by G. Ricigliano et al. (2025). We find the JWST spectrum can probe this mass down to  $\sim 10^{-4} M_{\odot}$ . However, the SUMO model is able to reproduce most of these lines without  $r$ -process elements. Since the exact strength and shape of features produced by the model do not match the observed spectrum, there is a possibility of blending of lines with  $r$ -process ions. This work shows that we need more observations of SN Ic-bl during the nebular phase and more models, including  $r$ -process ions, to separate the blending of lines, to answer definitively whether SN Ic-bl produces  $r$ -process elements or not.

To put the observed behavior of SN 2024abup in context with other transients, we compare NIR spectra of SN 2024abup with three other transients: SN 1998bw, AT 2017gfo, and GRB 230307A. The broad feature at  $2.1 \mu\text{m}$  has been attributed to the  $r$ -process line of

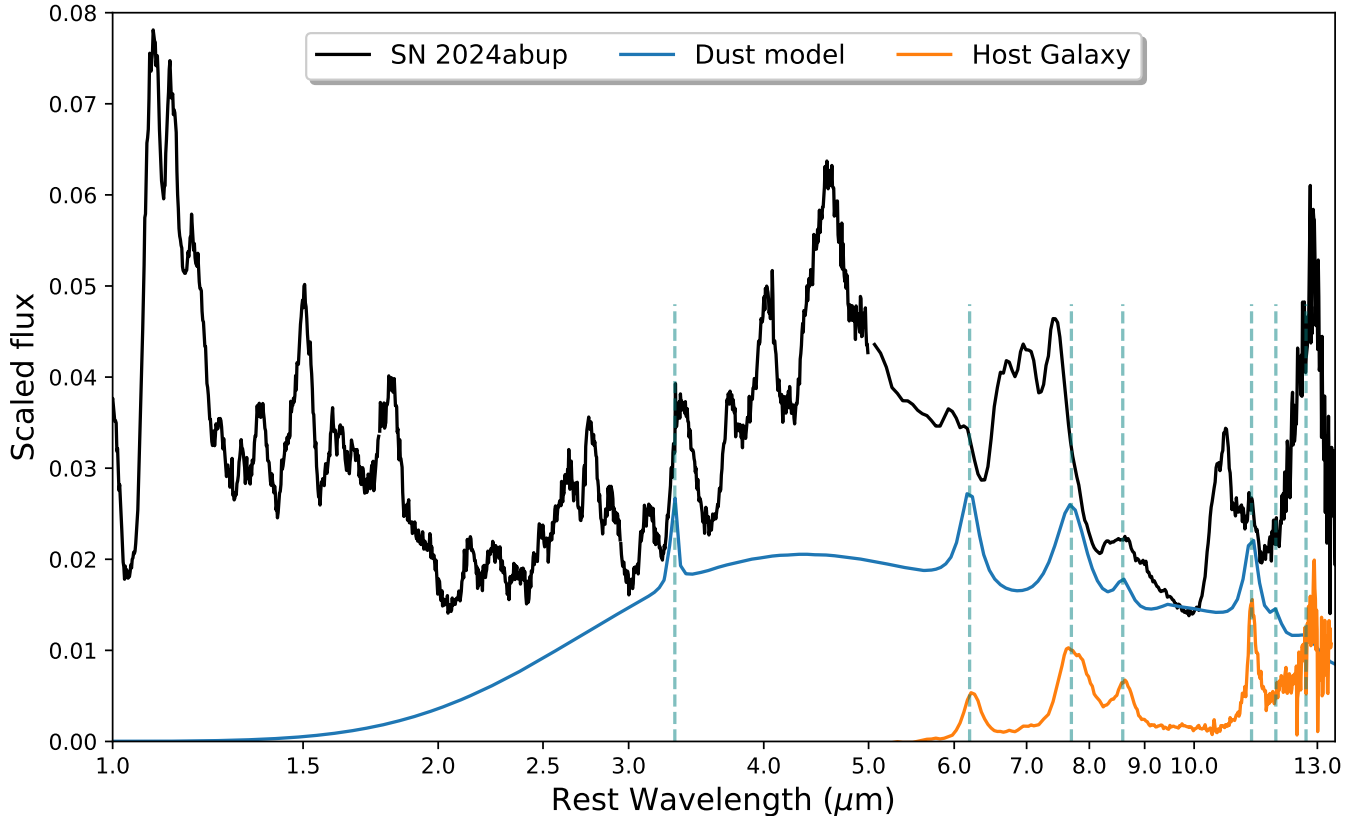


**Figure 10.** SN 2024abup spectrum (black) along with the model of graphite, silicate, and PAH contribution (blue) and the host galaxy (orange). The prominent PAH lines, contributed mainly by the host galaxy, are identified by dashed teal lines. There is a clear excess in the continuum of SN 2024abup compared to the host galaxy spectrum.

[Te III] in the case of AT 2017gfo and GRB 230307A. We see a feature at the same wavelength for SN 2024abup; however, the width of the feature is much smaller than in the case of AT 2017gfo and could be due to Mg II. This is a more favorable case for SN 2024abup because Mg lines are prominent at other wavelengths as well. We do note that in SN 2024abup, there is a possibility of blending of lines produced by both [Te III] and Mg II. Nonetheless, we do not see a clear sign of  $r$ -process elements in the NIR spectrum of SN 2024abup.

We observe a broad feature at  $\sim 4.5 \mu\text{m}$  which is produced by CO I as shown by a SUMO model. This is the first-ever detection of CO in any SN Ic-bl and one of the earliest for any CCSN. Since CO is a coolant that can effectively decrease the temperature of SN ejecta to be ideal for dust formation, the detection of this ion signifies that dust formation can commence. We estimate a CO mass of  $\sim 2 \times 10^{-5} M_{\odot}$  from the observed spectrum. Additionally, we observe some excess in the continuum in the MIR. This excess could be explained as dust heated by the SN, and is not likely due to host galaxy contamination. We find a combination of silicate and graphite dust of mass 0.05 and 0.009  $M_{\odot}$  heated to

temperatures of 300 K and 700 K, respectively, reproduces the observed excess in the continuum. We find a hint of dust formation in SN Ic-bl for the first time, and it could play an important role in producing dust in the early universe.

We also present a comparison of the JWST spectra of SN 2023dbc (Type Ic/Ib) and SN 2024abup obtained at similar epochs, finding many similarities between the two SNe. However, there are strong He I lines in SN 2023dbc, which are absent in SN 2024abup. This could indicate that the progenitor of SN 2024abup is more stripped of its He envelope than the progenitor of SN 2024abup. Additionally, we detect [Ar II] and [Ar III] lines in SN 2024abup, which are much weaker in SN 2023dbc. This could indicate that SN 2024abup is at a higher ionization state compared to SN 2023dbc. The CO feature seen in SN 2024abup is much more prominent than the feature seen in SN 2023dbc. Hence, there could be a small amount of CO in SN 2023dbc. These observed differences point to different levels of stripping and possibly dust production in the SN Ic-bl and SN Ic classes, which future observations should verify.

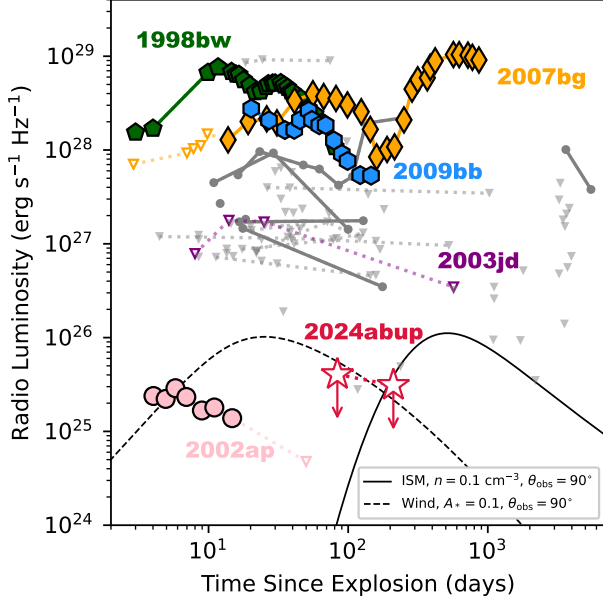


**Figure 11.** Radio light curve of SN 2024abup at frequencies shown in Table 3, shown alongside other well-studied SN Ic-bl for comparison: 1998bw (S. R. Kulkarni et al. 1998); 2002ap (E. Berger et al. 2002); 2003jd (A. M. Soderberg et al. 2006); 2007bg (P. Salas et al. 2013); 2009bb (A. M. Soderberg et al. 2010); detections and upper limits of several other SNe are from A. Soderberg (2007), A. Corsi et al. (2023), and G. Schroeder et al. (2025). The solid and dashed curves show the expected 6 GHz light curves generated using *VegasAfterglow* (Y. Wang et al. 2026) for a typical relativistic jet with energy  $E_{iso} = 10^{51}$  erg, initial Lorentz factor  $\Gamma_0 = 10^2$ , jet opening angle  $\theta_j = 0.2$ , electron power-law index  $p = 2.3$ , and microphysical parameters  $\epsilon_e = 0.1$  and  $\epsilon_B = 0.01$ . The solid curve assumes an ISM-like CSM with density  $n = 0.1 \text{ cm}^{-3}$ , while the dashed curve assumes a wind-like medium with  $A_* = 0.1$ , both for a maximally off-axis viewing angle of  $\theta_{obs} = 90^\circ$ . Our non-detections rule out these typical GRB-like jet models for any viewing angle more on-axis than  $\theta_{obs} = 90^\circ$ , implying that any relativistic jet in SN 2024abup if present, must be either less energetic than standard GRB jets or propagating through a significantly lower-density environment.

We search for an off-axis jet using radio observations with the VLA. We do not detect radio emission coincident with SN 2024abup and obtain a deep limit in our VLA radio observations. Here, non-detection in the radio for SN 2024abup could mean that the jet is not launched or pointed at a viewing angle not visible even in radio frequencies. Additionally, it could mean that there is no dense medium near the explosion.

This work shows the power of one JWST SN Ic-bl spectrum in furthering our understanding of chemical enrichment and dust formation from this class of transients. We do not detect any clear sign of  $r$ -process

element production in SN 2024abup. Future observations in the IR during nebular epochs could provide a clearer answer to the question if collapsars could produce  $r$ -process elements. However, it is clear that SN Ic-bl could produce dust, and more work needs to be done to constrain the amount of dust produced by these transients.

## ACKNOWLEDGMENTS

The work presented here is based on observations made with the NASA/ESA/CSA JWST as part of program #06803. We thank William Januszewski for the help with observation scheduling. The data were obtained from the Mikulski Archive for Space Telescopes at the Space Telescope Science Institute (STScI), which is operated by the Association of Universities for Research in Astronomy (AURA), Inc., under National Aeronautics and Space Administration (NASA) contract NAS 5-03127 for JWST. Support for this program at the University of Arizona was provided by NASA through grants JWST-GO-06803.003.

MS acknowledges funding from the Australian Research Council (ARC) Centre of Excellence CE230100016. Time-domain research by the University of Arizona team and D.J.S. is supported by National Science Foundation (NSF) grants 2308181, 2407566, and 2432036. The research by Y.D., S.V., N.M., and E.H. is supported by NSF grant AST-2008108.

This work makes use of data from the Las Cumbres Observatory global telescope network. The LCO team is supported by NSF grants AST-1911225 and AST-1911151.

K.A.B. is supported by an LSSTC Catalyst Fellowship; this publication was thus made possible through the support of Grant 62192 from the John Templeton Foundation to LSSTC. The opinions expressed in this publication are those of the authors and do not necessarily reflect the views of LSSTC or the John Templeton Foundation.

M.M. acknowledges support in part from ADAP program grant No. 80NSSC22K0486, from the NSF grant AST-2206657 and from the National Science Foundation under Cooperative Agreement 2421782 and the Simons Foundation grant MPS-AI-00010515 awarded to the NSF-Simons AI Institute for Cosmic Origins (CosmicAI), <https://www.cosmicai.org/>.

A.J. acknowledges funding by the Swedish Research Council (Grant 2018-03799). The SUMO computations in this work were enabled by resources provided by the Swedish National Infrastructure for Computing (SNIC), the National Academic Infrastructure for Supercom-

puting in Sweden (NAISS), and at the Paralleldatorcentrum (PDC) Center for High Performance Computing, Royal Institute of Technology (KTH), partially funded by the Swedish Research Council through grant agreements nos 2022- 06725 and 2018-05973.

This research has made use of the NASA Astrophysics Data System (ADS) Bibliographic Services, and the NASA/IPAC Infrared Science Archive (IRSA), which is funded by the National Aeronautics and Space Administration and operated by the California Institute of Technology. This work made use of data supplied by the UK Swift Science Data Centre at the University of Leicester. BM acknowledges support from the ARC through Discovery Projects DP240101786 and DP260104967. S.W.J. gratefully acknowledges support from a Guggenheim Fellowship.

## APPENDIX

### A. CORNER PLOT

### B. *R*-PROCESS LINES

Figure B.1 shows the JWST spectrum of SN 2024abup covering the wavelength range from 1 to 6.5  $\mu\text{m}$  with all the prominent *r*-process lines predicted by G. Riciigliano et al. (2025) as shown in their table 3. All of the lines are forbidden lines from heavy elements.

### C. RADIO OBSERVATIONS

In Table 3, we present the summary of VLA observations performed for SN 2024abup in two different epochs. We present the upper limit for our non-detection in different frequency ranges. This deep limit, along with other well-studied SNe Ic-BL in the radio, are presented in Figure 11. We see that if the radio emission from SN 2024abup was similar to other SN Ic-bl, then we should have detected it.

### D. SUMO MODEL

In this appendix, we will provide a more detailed description of the SUMO spectral modeling effort presented in Section 5.1. As mentioned there, we selected the  $M_{\text{He, i}} = 12.0 M_{\odot}$  model from S. E. Woosley (2019) and T. Ertl et al. (2020) as our base ejecta model. This model was cut up into different compositional zones following the methodology described in S. Barmantloo

*Facilities:* JWST(NIRSpec+MIRI), LCOGT, Swift (UVOT), VLA

*Software:* Astropy (Astropy Collaboration et al. 2013; A. M. Price-Whelan et al. 2018; Astropy Collaboration et al. 2022), Photutils (L. Bradley et al. 2019), Panacea, BANZAI (C. McCully et al. 2018), Light Curve Fitting (G. Hosseinzadeh & S. Gomez 2020), Matplotlib (J. D. Hunter 2007), Numpy (C. R. Harris et al. 2020), Scipy (P. Virtanen et al. 2020), IRAF (D. Tody 1986, 1993), lcogtsnpipe (S. Valenti et al. 2016)

et al. (2024). These zones are dubbed the Fe/He, Si/S, O/Si/S, O/Ne/Mg, O/C, and C/O zones. The O/C + C/O split (not present in S. Barmantloo et al. 2024) was not only a better empirical description of the compositional profiles (see Figure 6), it was also found to be essential for proper (CO) molecule formation in SUMO, as a single O/C zone would be too polluted by  $\text{He}^+$ , causing too efficient destruction of CO molecules (W. Liu et al. 1992; S. Liljegren et al. 2020). To obtain a model completely free of a helium envelope, the C/O zone was cut off as soon as the mass abundance of helium surpassed 0.2 (removing the  $\sim 2.5\%$  fastest moving ejecta). Additionally, the  $^{56}\text{Ni}$  mass of the model was increased to  $0.0791 M_{\odot}$  (following L. Dessart et al. 2021; see their table A.2) by simply increasing the mass of  $^{56}\text{Ni}$  in the Fe/He zone by the required amount, adjusting all other mass abundances so that all other elemental masses are conserved.

With the compositional zones defined, we now macroscopically mix the ejecta, randomly distributing 1000 ‘clumps’ per compositional zone within a sphere at radii ranging from  $R = 0$  to  $R = V_{\text{core}}t$ .<sup>30</sup> Following earlier works with SUMO (e.g., A. Jerkstrand et al. 2015), we assume the Fe/He and Si/S zones to expand due to radioactive heating (M. Herant & W. Benz 1991). As in A. Jerkstrand et al. (2015), we assume an expansion such that  $\rho_{\text{FeHE}} = \rho_{\text{SiS}}/10 = \rho_{\text{other zones}}/30$ .

## REFERENCES

Alexander, K. D., Berger, E., Fong, W., et al. 2017, ApJL, 848, L21, doi: 10.3847/2041-8213/aa905d

<sup>30</sup> Here,  $V_{\text{core}}$  is the outer velocity of the C/O zone (see Table 4).

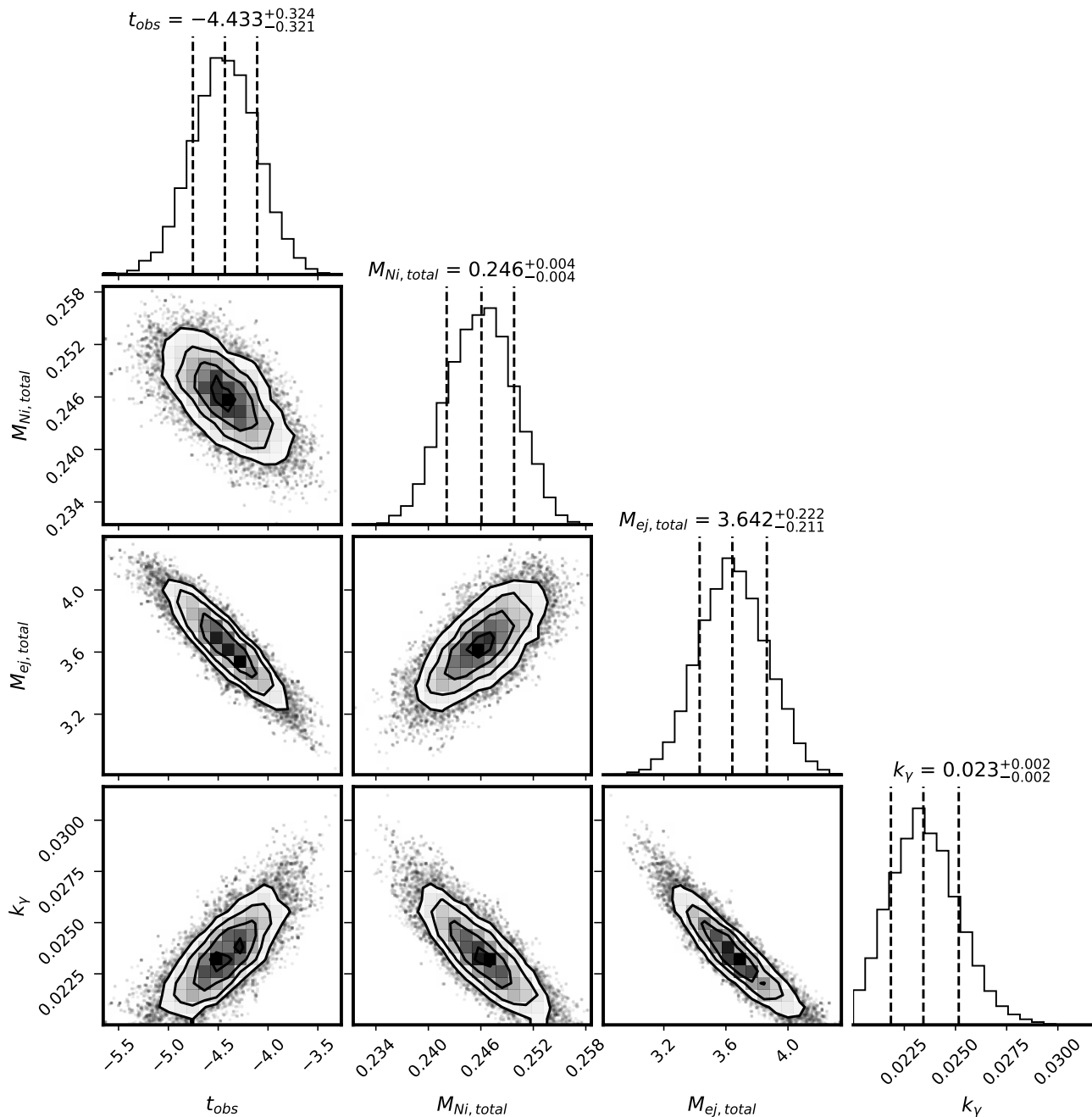


**Figure A.1.** The corner plot for the fit using analytic models from [W. D. Arnett \(1982\)](#) and [S. Valenti et al. \(2008\)](#).

Anand, S., Barnes, J., Yang, S., et al. 2024, *ApJ*, 962, 68,  
doi: [10.3847/1538-4357/ad11df](https://doi.org/10.3847/1538-4357/ad11df)

Andreoni, I., Ackley, K., Cooke, J., et al. 2017, *PASA*, 34,  
e069, doi: [10.1017/pasa.2017.65](https://doi.org/10.1017/pasa.2017.65)

Arcavi, I., Hosseinzadeh, G., Howell, D. A., et al. 2017,  
*Nature*, 551, 64, doi: [10.1038/nature24291](https://doi.org/10.1038/nature24291)

Arnett, W. D. 1982, *ApJ*, 253, 785, doi: [10.1086/159681](https://doi.org/10.1086/159681)

Arunachalam, P., Macias, P., & Foley, R. J. 2025, arXiv  
e-prints, arXiv:2510.16121,  
doi: [10.48550/arXiv.2510.16121](https://doi.org/10.48550/arXiv.2510.16121)

Astropy Collaboration, Robitaille, T. P., Tollerud, E. J.,  
et al. 2013, *A&A*, 558, A33,  
doi: [10.1051/0004-6361/201322068](https://doi.org/10.1051/0004-6361/201322068)

Astropy Collaboration, Price-Whelan, A. M., Lim, P. L.,  
et al. 2022, *ApJ*, 935, 167, doi: [10.3847/1538-4357/ac7c74](https://doi.org/10.3847/1538-4357/ac7c74)

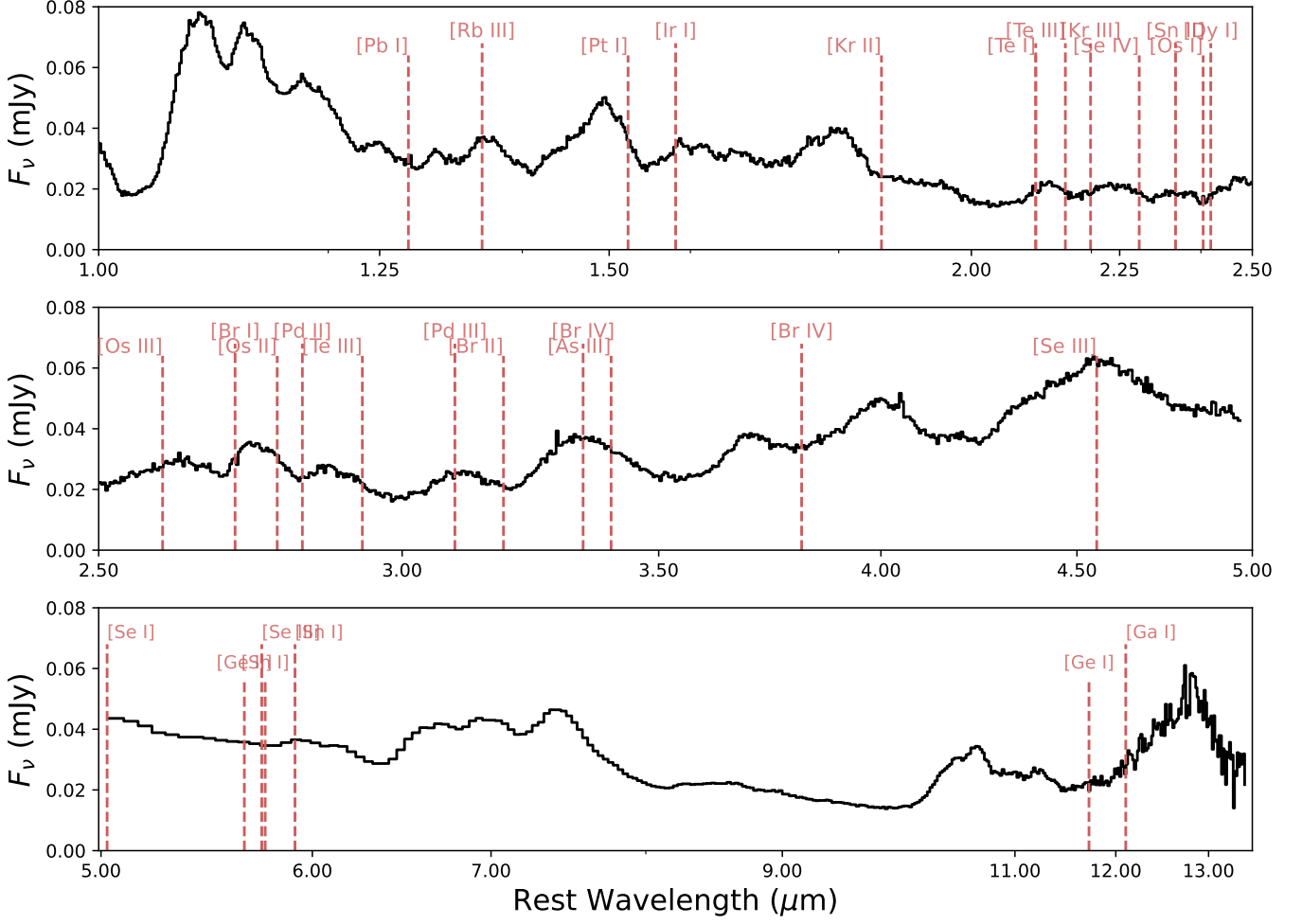


**Figure B.1.** The SN 2024abup JWST spectrum overlaid with all the prominent  $r$ -process lines identified and presented in Table 3 in G. Ricigliano et al. (2025) (red dashed lines).

**Table 3.** Summary of VLA Observations. Non-detections are reported as  $3\sigma$  upper limits.

Date (UTC)	MJD	Configuration	Phase (d)	$\nu$ (GHz)	$F_\nu$ (mJy)
2025-02-14	60720	A→D	84	1.52	<0.16
2025-02-14	60720	A→D	84	3.0	<0.10
2025-02-14	60720	A→D	84	6.0	<0.06
2025-02-14	60720	A→D	84	10.0	<0.06
2025-06-21	60848	C	211	1.52	<0.22
2025-06-21	60848	C	211	3.0	<0.11
2025-06-21	60848	C	211	6.0	<0.05
2025-06-21	60848	C	211	10.0	<0.05

Parameter	Value
$E_{\text{kin}}$	0.81 B
$M_{\text{preSN}}$	7.24 $M_{\odot}$
$M_{\text{ej}}$	5.18 $M_{\odot}$
$M_{56\text{Ni}}$	0.0791 $M_{\odot}$
$V_{\text{core}}$	8 547 km s <sup>-1</sup>

**Table 4.** Summary table of the properties of the ejecta model used to simulate the SUMO model spectrum presented in Figure 6. This ejecta model is an adoption of the  $M_{\text{He}, i} = 12.0 M_{\odot}$  model from S. E. Woosley (2019) and T. Ertl et al. (2020) (see text)

Balcon, C. 2024, Transient Name Server Classification Report, 2024-4655, 1

Barentloo, S., Jerkstrand, A., Iwamoto, K., et al. 2024, MNRAS, 533, 1251, doi: [10.1093/mnras/stae1811](https://doi.org/10.1093/mnras/stae1811)

Barnes, J., & Metzger, B. D. 2022, ApJL, 939, L29, doi: [10.3847/2041-8213/ac9b41](https://doi.org/10.3847/2041-8213/ac9b41)

Berger, E., Kulkarni, S. R., & Chevalier, R. A. 2002, ApJL, 577, L5, doi: [10.1086/344045](https://doi.org/10.1086/344045)

Bradley, L., Sipőcz, B., Robitaille, T., et al. 2019, astropy/photutils: v0.6, doi: [10.5281/zenodo.2533376](https://doi.org/10.5281/zenodo.2533376)

Breeveld, A. A., Curran, P. A., Hoversten, E. A., et al. 2010, MNRAS, 406, 1687, doi: [10.1111/j.1365-2966.2010.16832.x](https://doi.org/10.1111/j.1365-2966.2010.16832.x)

Brown, T. M., Baliber, N., Bianco, F. B., et al. 2013, PASP, 125, 1031, doi: [10.1086/673168](https://doi.org/10.1086/673168)

Cano, Z., Wang, S.-Q., Dai, Z.-G., & Wu, X.-F. 2017, Advances in Astronomy, 2017, 8929054, doi: [10.1155/2017/892905410.48550/arXiv.1604.03549](https://doi.org/10.1155/2017/892905410.48550/arXiv.1604.03549)

CASA Team, Bean, B., Bhatnagar, S., et al. 2022, PASP, 134, 114501, doi: [10.1088/1538-3873/ac9642](https://doi.org/10.1088/1538-3873/ac9642)

Chabrier, G. 2003, PASP, 115, 763, doi: [10.1086/376392](https://doi.org/10.1086/376392)

Chen, T.-W., Aryan, A., Yang, S., et al. 2026, arXiv e-prints, arXiv:2606.10009, doi: [10.48550/arXiv.2606.10009](https://doi.org/10.48550/arXiv.2606.10009)

Cherchneff, I., Talbi, D., & Cernicharo, J. 2026, A&A, 708, A76, doi: [10.1051/0004-6361/202557490](https://doi.org/10.1051/0004-6361/202557490)

Corsi, A., Gal-Yam, A., Kulkarni, S. R., et al. 2016, ApJ, 830, 42, doi: [10.3847/0004-637X/830/1/42](https://doi.org/10.3847/0004-637X/830/1/42)

Corsi, A., Ho, A. Y. Q., Cenko, S. B., et al. 2023, ApJ, 953, 179, doi: [10.3847/1538-4357/acd3f2](https://doi.org/10.3847/1538-4357/acd3f2)

Coulter, D. A., Foley, R. J., Kilpatrick, C. D., et al. 2017, Science, 358, 1556, doi: [10.1126/science.aap9811](https://doi.org/10.1126/science.aap9811)

Covino, S., Wiersema, K., Fan, Y. Z., et al. 2017, Nature Astronomy, 1, 791, doi: [10.1038/s41550-017-0285-z](https://doi.org/10.1038/s41550-017-0285-z)

Cowperthwaite, P. S., Berger, E., Villar, V. A., et al. 2017, ApJL, 848, L17, doi: [10.3847/2041-8213/aa8fc7](https://doi.org/10.3847/2041-8213/aa8fc7)

Dell’Agli, F., Di Criscienzo, M., Ventura, P., et al. 2018, MNRAS, 479, 5035, doi: [10.1093/mnras/sty1614](https://doi.org/10.1093/mnras/sty1614)

Dessart, L., Hillier, D. J., Sukhbold, T., Woosley, S. E., & Janka, H.-T. 2021, A&A, 656, A61, doi: [10.1051/0004-6361/202141927](https://doi.org/10.1051/0004-6361/202141927)

Drout, M. R., Soderberg, A. M., Gal-Yam, A., et al. 2011, ApJ, 741, 97, doi: [10.1088/0004-637X/741/2/9710.48550/arXiv.1011.4959](https://doi.org/10.1088/0004-637X/741/2/9710.48550/arXiv.1011.4959)

Drout, M. R., Piro, A. L., Shappee, B. J., et al. 2017, Science, 358, 1570, doi: [10.1126/science.aaq0049](https://doi.org/10.1126/science.aaq0049)

Dwek, E., & Cherchneff, I. 2011, ApJ, 727, 63, doi: [10.1088/0004-637X/727/2/63](https://doi.org/10.1088/0004-637X/727/2/63)

Ertl, T., Woosley, S. E., Sukhbold, T., & Janka, H.-T. 2020, ApJ, 890, 51, doi: [10.3847/1538-4357/ab6458](https://doi.org/10.3847/1538-4357/ab6458)

Evans, P. A., Cenko, S. B., Kennea, J. A., et al. 2017, Science, 358, 1565, doi: [10.1126/science.aap9580](https://doi.org/10.1126/science.aap9580)

Fujibayashi, S., Shibata, M., Wanajo, S., et al. 2020, PhRvD, 101, 083029, doi: [10.1103/PhysRevD.101.083029](https://doi.org/10.1103/PhysRevD.101.083029)

Fulton, M. D., Smartt, S. J., Rhodes, L., et al. 2023, arXiv e-prints, arXiv:2301.11170, <https://arxiv.org/abs/2301.11170>

Gaskell, C. M., Cappellaro, E., Dinerstein, H. L., et al. 1986, ApJL, 306, L77, doi: [10.1086/184709](https://doi.org/10.1086/184709)

Gehrels, N., Chincarini, G., Giommi, P., et al. 2004, ApJ, 611, 1005, doi: [10.1086/422091](https://doi.org/10.1086/422091)

Gehrz, R. 1989, in IAU Symposium, Vol. 135, Interstellar Dust, ed. L. J. Allamandola & A. G. G. M. Tielens, 445

Gillanders, J. H., & Smartt, S. J. 2025, MNRAS, 538, 1663, doi: [10.1093/mnras/staf287](https://doi.org/10.1093/mnras/staf287)

Goldstein, A., Veres, P., Burns, E., et al. 2017, ApJL, 848, L14, doi: [10.3847/2041-8213/aa8f41](https://doi.org/10.3847/2041-8213/aa8f41)

Gordon, A. J., Ferguson, A. M. N., & Mann, R. G. 2024, MNRAS, 534, 1459, doi: [10.1093/mnras/stae2169](https://doi.org/10.1093/mnras/stae2169)

Grichener, A. 2025, Ap&SS, 370, 11, doi: [10.1007/s10509-025-04402-1](https://doi.org/10.1007/s10509-025-04402-1)

Haggard, D., Nynka, M., Ruan, J. J., et al. 2017, ApJL, 848, L25, doi: [10.3847/2041-8213/aa8ede](https://doi.org/10.3847/2041-8213/aa8ede)

Harris, C. R., Millman, K. J., van der Walt, S. J., et al. 2020, Nature, 585, 357, doi: [10.1038/s41586-020-2649-2](https://doi.org/10.1038/s41586-020-2649-2)

Hensley, B. S., & Draine, B. T. 2023, ApJ, 948, 55, doi: [10.3847/1538-4357/acc4c2](https://doi.org/10.3847/1538-4357/acc4c2)

Herant, M., & Benz, W. 1991, ApJL, 370, L81, doi: [10.1086/185982](https://doi.org/10.1086/185982)

Hosseinzadeh, G., Bostroem, K. A., & Gomez, S. 2023, Light Curve Fitting v0.9.0., Zenodo, doi: [10.5281/zenodo.8049154](https://doi.org/10.5281/zenodo.8049154)

Hosseinzadeh, G., & Gomez, S. 2020, Light Curve Fitting, v0.2.0, Zenodo Zenodo, doi: [10.5281/zenodo.4312178](https://doi.org/10.5281/zenodo.4312178)

Hotokezaka, K., Tanaka, M., Kato, D., & Gaigalas, G. 2022, MNRAS, 515, L89, doi: [10.1093/mnras/515/l89](https://doi.org/10.1093/mnras/515/l89)

Hunter, J. D. 2007, Computing in Science and Engineering, 9, 90, doi: [10.1109/MCSE.2007.55](https://doi.org/10.1109/MCSE.2007.55)

- Issa, D., Gottlieb, O., Metzger, B. D., et al. 2025, *ApJL*, 985, L26, doi: [10.3847/2041-8213/adc694](https://doi.org/10.3847/2041-8213/adc694)
- Japelj, J., Vergani, S. D., Salvaterra, R., et al. 2018, *A&A*, 617, A105, doi: [10.1051/0004-6361/201833209](https://doi.org/10.1051/0004-6361/201833209)
- Jerkstrand, A. 2017, in *Handbook of Supernovae*, ed. A. W. Alsabti & P. Murdin, 795, doi: [10.1007/978-3-319-21846-5\\_29](https://doi.org/10.1007/978-3-319-21846-5_29)
- Jerkstrand, A., Ergon, M., Smartt, S. J., et al. 2015, *A&A*, 573, A12, doi: [10.1051/0004-6361/201423983](https://doi.org/10.1051/0004-6361/201423983)
- Jerkstrand, A., Fransson, C., & Kozma, C. 2011, *A&A*, 530, A45, doi: [10.1051/0004-6361/201015937](https://doi.org/10.1051/0004-6361/201015937)
- Jerkstrand, A., Fransson, C., Maguire, K., et al. 2012, *A&A*, 546, A28, doi: [10.1051/0004-6361/201219528](https://doi.org/10.1051/0004-6361/201219528)
- Ji, A. P., Frebel, A., Chiti, A., & Simon, J. D. 2016, *Nature*, 531, 610, doi: [10.1038/nature17425](https://doi.org/10.1038/nature17425)
- Just, O., Bauswein, A., Ardevol Pulpillo, R., Goriely, S., & Janka, H. T. 2015, *MNRAS*, 448, 541, doi: [10.1093/mnras/stv009](https://doi.org/10.1093/mnras/stv009)
- Kalinova, V., Colombo, D., Sánchez, S. F., et al. 2021, *A&A*, 648, A64, doi: [10.1051/0004-6361/202039896](https://doi.org/10.1051/0004-6361/202039896)
- Kasliwal, M. M., Nakar, E., Singer, L. P., et al. 2017, *Science*, 358, 1559, doi: [10.1126/science.aap9455](https://doi.org/10.1126/science.aap9455)
- Kasliwal, M. M., Kasen, D., Lau, R. M., et al. 2022, *MNRAS*, 510, L7, doi: [10.1093/mnrasl/slz007](https://doi.org/10.1093/mnrasl/slz007)
- Kulkarni, S. R., Frail, D. A., Wieringa, M. H., et al. 1998, *Nature*, 395, 663, doi: [10.1038/27139](https://doi.org/10.1038/27139)
- Laplace, E., Justham, S., Renzo, M., et al. 2021, *A&A*, 656, A58, doi: [10.1051/0004-6361/202140506](https://doi.org/10.1051/0004-6361/202140506)
- Laporte, N., Ellis, R. S., Boone, F., et al. 2017, *ApJL*, 837, L21, doi: [10.3847/2041-8213/aa62aa](https://doi.org/10.3847/2041-8213/aa62aa)
- Levan, A. J., Gompertz, B. P., Salafia, O. S., et al. 2024, *Nature*, 626, 737, doi: [10.1038/s41586-023-06759-1](https://doi.org/10.1038/s41586-023-06759-1)
- Li, W., Leaman, J., Chornock, R., et al. 2011, *MNRAS*, 412, 1441, doi: [10.1111/j.1365-2966.2011.18160.x](https://doi.org/10.1111/j.1365-2966.2011.18160.x)
- Lidman, C., Rauf, L., Auchettl, K., et al. 2024, *Transient Name Server Classification Report*, 2024-4668, 1
- Liljegren, S., Jerkstrand, A., & Grumer, J. 2020, *A&A*, 642, A135, doi: [10.1051/0004-6361/202038116](https://doi.org/10.1051/0004-6361/202038116)
- Liu, W., Dalgarno, A., & Lepp, S. 1992, *ApJ*, 396, 679, doi: [10.1086/171749](https://doi.org/10.1086/171749)
- MacFadyen, A. I., & Woosley, S. E. 1999, *ApJ*, 524, 262, doi: [10.1086/307790](https://doi.org/10.1086/307790)
- Margutti, R., & Chornock, R. 2021, *ARA&A*, 59, 155, doi: [10.1146/annurev-astro-112420-030742](https://doi.org/10.1146/annurev-astro-112420-030742)
- Margutti, R., Berger, E., Fong, W., et al. 2017, *ApJL*, 848, L20, doi: [10.3847/2041-8213/aa9057](https://doi.org/10.3847/2041-8213/aa9057)
- McCully, C., Volgenau, N. H., Harbeck, D.-R., et al. 2018, in *Society of Photo-Optical Instrumentation Engineers (SPIE) Conference Series*, Vol. 10707, *Software and Cyberinfrastructure for Astronomy V*, ed. J. C. Guzman & J. Ibsen, 107070K, doi: [10.1117/12.2314340](https://doi.org/10.1117/12.2314340)
- McMullin, J. P., Waters, B., Schiebel, D., Young, W., & Golap, K. 2007, in *Astronomical Society of the Pacific Conference Series*, Vol. 376, *Astronomical Data Analysis Software and Systems XVI*, ed. R. A. Shaw, F. Hill, & D. J. Bell, 127
- Medler, K., Ashall, C., Hoefflich, P., et al. 2025, *ApJ*, 993, 191, doi: [10.3847/1538-4357/ae0736](https://doi.org/10.3847/1538-4357/ae0736)
- Mera, T., Ashall, C., Hoefflich, P., et al. 2026, *ApJ*, 997, 330, doi: [10.3847/1538-4357/ae317e](https://doi.org/10.3847/1538-4357/ae317e)
- Milisavljevic, D., Margutti, R., Parrent, J. T., et al. 2015, *ApJ*, 799, 51, doi: [10.1088/0004-637X/799/1/51](https://doi.org/10.1088/0004-637X/799/1/51)
- Miller, J. M., Sprouse, T. M., Fryer, C. L., et al. 2020, *ApJ*, 902, 66, doi: [10.3847/1538-4357/abb4e3](https://doi.org/10.3847/1538-4357/abb4e3)
- Modjaz, M., Gutiérrez, C. P., & Arcavi, I. 2019, *Nature Astronomy*, 3, 717, doi: [10.1038/s41550-019-0856-2](https://doi.org/10.1038/s41550-019-0856-2)
- Modjaz, M., Liu, Y. Q., Bianco, F. B., & Graur, O. 2016, *ApJ*, 832, 108, doi: [10.3847/0004-637X/832/2/10810.48550/arXiv.1509.07124](https://doi.org/10.3847/0004-637X/832/2/10810.48550/arXiv.1509.07124)
- Modjaz, M., Bianco, F. B., Siwek, M., et al. 2020, *ApJ*, 892, 153, doi: [10.3847/1538-4357/ab418510.48550/arXiv.1901.00872](https://doi.org/10.3847/1538-4357/ab418510.48550/arXiv.1901.00872)
- Naidu, R. P., Ji, A. P., Conroy, C., et al. 2022, *ApJL*, 926, L36, doi: [10.3847/2041-8213/ac5589](https://doi.org/10.3847/2041-8213/ac5589)
- Nanni, A., Romano, M., Donevski, D., et al. 2025, *ApJL*, 988, L5, doi: [10.3847/2041-8213/ade2e5](https://doi.org/10.3847/2041-8213/ade2e5)
- Nicholl, M., Guillochon, J., & Berger, E. 2017, *ApJ*, 850, 55, doi: [10.3847/1538-4357/aa9334](https://doi.org/10.3847/1538-4357/aa9334)
- Nomoto, K. I., Iwamoto, K., & Suzuki, T. 1995, *PhR*, 256, 173, doi: [10.1016/0370-1573\(94\)00107-E](https://doi.org/10.1016/0370-1573(94)00107-E)
- Papish, O., Soker, N., & Bukay, I. 2015, *MNRAS*, 449, 288, doi: [10.1093/mnras/stv345](https://doi.org/10.1093/mnras/stv345)
- Park, S. H., Rho, J., Yoon, S.-C., et al. 2025, *A&A*, 703, A227, doi: [10.1051/0004-6361/202555244](https://doi.org/10.1051/0004-6361/202555244)
- Patat, F., Cappellaro, E., Danziger, J., et al. 2001, *ApJ*, 555, 900, doi: [10.1086/321526](https://doi.org/10.1086/321526)
- Patel, A., Metzger, B. D., Cehula, J., et al. 2025, *ApJL*, 984, L29, doi: [10.3847/2041-8213/adc9b0](https://doi.org/10.3847/2041-8213/adc9b0)
- Pian, E., D'Avanzo, P., Benetti, S., et al. 2017, *Nature*, 551, 67, doi: [10.1038/nature24298](https://doi.org/10.1038/nature24298)
- Podsiadlowski, P., Hsu, J. J. L., Joss, P. C., & Ross, R. R. 1993, *Nature*, 364, 509, doi: [10.1038/364509a0](https://doi.org/10.1038/364509a0)
- Price-Whelan, A. M., Sipőcz, B. M., Günther, H. M., et al. 2018, *AJ*, 156, 123, doi: [10.3847/1538-3881/aabc4f](https://doi.org/10.3847/1538-3881/aabc4f)
- Rastinejad, J. C., Fong, W., Levan, A. J., et al. 2024, *ApJ*, 968, 14, doi: [10.3847/1538-4357/ad409c](https://doi.org/10.3847/1538-4357/ad409c)

- Rastinejad, J. C., Levan, A. J., Jonker, P. G., et al. 2025, *ApJL*, 988, L13, doi: [10.3847/2041-8213/ade7f9](https://doi.org/10.3847/2041-8213/ade7f9)
- Ravi, A. P., Rho, J., Park, S., et al. 2023, *ApJ*, 950, 14, doi: [10.3847/1538-4357/acddc](https://doi.org/10.3847/1538-4357/acddc)
- Renzo, M., Gottlieb, O., Chan, H. S., et al. 2026, arXiv e-prints, arXiv:2606.21824. <https://arxiv.org/abs/2606.21824>
- Rho, J., Evans, A., Geballe, T. R., et al. 2021, *ApJ*, 908, 232, doi: [10.3847/1538-4357/abd850](https://doi.org/10.3847/1538-4357/abd850)
- Ricigliano, G., Hotokezaka, K., & Arcones, A. 2025, *MNRAS*, doi: [10.1093/mnras/staf1577](https://doi.org/10.1093/mnras/staf1577)
- Roming, P. W. A., Kennedy, T. E., Mason, K. O., et al. 2005, *SSRv*, 120, 95, doi: [10.1007/s11214-005-5095-4](https://doi.org/10.1007/s11214-005-5095-4)
- Sahu, D. K., Tanaka, M., Anupama, G. C., Gurugubelli, U. K., & Nomoto, K. 2009, *ApJ*, 697, 676, doi: [10.1088/0004-637X/697/1/676](https://doi.org/10.1088/0004-637X/697/1/676)
- Salas, P., Bauer, F. E., Stockdale, C., & Prieto, J. L. 2013, *MNRAS*, 428, 1207, doi: [10.1093/mnras/sts104](https://doi.org/10.1093/mnras/sts104)
- Sarangi, A., Dwek, E., & Arendt, R. G. 2018, *ApJ*, 859, 66, doi: [10.3847/1538-4357/aabfc3](https://doi.org/10.3847/1538-4357/aabfc3)
- Savchenko, V., Ferrigno, C., Kuulkers, E., et al. 2017, *ApJL*, 848, L15, doi: [10.3847/2041-8213/aa8f94](https://doi.org/10.3847/2041-8213/aa8f94)
- Schlafly, E. F., & Finkbeiner, D. P. 2011, *ApJ*, 737, 103, doi: [10.1088/0004-637X/737/2/103](https://doi.org/10.1088/0004-637X/737/2/103)
- Schneider, R., & Maiolino, R. 2024, *A&A Rv*, 32, 2, doi: [10.1007/s00159-024-00151-2](https://doi.org/10.1007/s00159-024-00151-2)
- Schroeder, G., Ho, A. Y. Q., Dastidar, R. G., et al. 2025, *ApJ*, 995, 61, doi: [10.3847/1538-4357/ae129b](https://doi.org/10.3847/1538-4357/ae129b)
- Shahbandeh, M., Ashall, C., Baade, D., et al. 2023, Near- and Mid-IR Observations to Probe Dust Formation in the Remarkably Nearby Stripped-Envelope Supernova 2023dbc,, JWST Proposal. Cycle 1, ID. #4436
- Shivvers, I., Modjaz, M., Zheng, W., et al. 2017, *PASP*, 129, 054201, doi: [10.1088/1538-3873/aa54a6](https://doi.org/10.1088/1538-3873/aa54a6)
- Shrestha, M., Alexander, K. D., Andrews, J., et al. 2024, NIR+MIR Spectroscopy of the Nearby Broad Line Type Ic SN 2024abup: r-process, Dust and Explosion Physics,, JWST Proposal. Cycle 3, ID. #6803
- Siebert, M. R., DeCoursey, C., Coulter, D. A., et al. 2024, *ApJL*, 972, L13, doi: [10.3847/2041-8213/ad6c32](https://doi.org/10.3847/2041-8213/ad6c32)
- Siegel, D. M., Agarwal, A., Barnes, J., et al. 2022, *ApJ*, 941, 100, doi: [10.3847/1538-4357/ac8d04](https://doi.org/10.3847/1538-4357/ac8d04)
- Siegel, D. M., Barnes, J., & Metzger, B. D. 2019, *Nature*, 569, 241, doi: [10.1038/s41586-019-1136-0](https://doi.org/10.1038/s41586-019-1136-0)
- Smartt, S. J. 2009, *ARA&A*, 47, 63, doi: [10.1146/annurev-astro-082708-10173710.48550/arXiv.0908.0700](https://doi.org/10.1146/annurev-astro-082708-10173710.48550/arXiv.0908.0700)
- Smartt, S. J., Chen, T. W., Jerkstrand, A., et al. 2017, *Nature*, 551, 75, doi: [10.1038/nature24303](https://doi.org/10.1038/nature24303)
- Smith, K. W., Smartt, S. J., Young, D. R., et al. 2020, *PASP*, 132, 085002, doi: [10.1088/1538-3873/ab936e](https://doi.org/10.1088/1538-3873/ab936e)
- Soares-Santos, M., Holz, D. E., Annis, J., et al. 2017, *ApJL*, 848, L16, doi: [10.3847/2041-8213/aa9059](https://doi.org/10.3847/2041-8213/aa9059)
- Sobolev, V. V. 1957, *Soviet Ast.*, 1, 678
- Soderberg, A. 2007, PhD thesis, California Institute of Technology
- Soderberg, A. M., Nakar, E., Berger, E., & Kulkarni, S. R. 2006, *ApJ*, 638, 930, doi: [10.1086/499121](https://doi.org/10.1086/499121)
- Soderberg, A. M., Chakraborti, S., Pignata, G., et al. 2010, *Nature*, 463, 513, doi: [10.1038/nature08714](https://doi.org/10.1038/nature08714)
- Spyromilio, J., Meikle, W. P. S., Learner, R. C. M., & Allen, D. A. 1989, in *Infrared Spectroscopy in Astronomy*, ed. E. Böhm-Vitense, 381
- Srinivasaragavan, G. P., Yang, S., Anand, S., et al. 2024, *ApJ*, 976, 71, doi: [10.3847/1538-4357/ad7fde](https://doi.org/10.3847/1538-4357/ad7fde)
- Stoppa, F., & Smartt, S. J. 2026, *Monthly Notices of the Royal Astronomical Society*, 549, stag1066, doi: [10.1093/mnras/stag1066](https://doi.org/10.1093/mnras/stag1066)
- Stritzinger, M. D., Taddia, F., Burns, C. R., et al. 2018, *A&A*, 609, A135, doi: [10.1051/0004-6361/201730843](https://doi.org/10.1051/0004-6361/201730843)
- Taddia, F., Sollerman, J., Fremling, C., et al. 2019, *A&A*, 621, A71, doi: [10.1051/0004-6361/201834429](https://doi.org/10.1051/0004-6361/201834429)
- Tanvir, N. R., Levan, A. J., González-Fernández, C., et al. 2017, *ApJL*, 848, L27, doi: [10.3847/2041-8213/aa90b6](https://doi.org/10.3847/2041-8213/aa90b6)
- The LIGO Scientific Collaboration, the Virgo Collaboration, & the KAGRA Collaboration. 2026, arXiv e-prints, arXiv:2605.27226, doi: [10.48550/arXiv.2605.27226](https://doi.org/10.48550/arXiv.2605.27226)
- The LIGO Scientific Collaboration, the Virgo Collaboration, the KAGRA Collaboration, et al. 2025, arXiv e-prints, arXiv:2508.18083, doi: [10.48550/arXiv.2508.18083](https://doi.org/10.48550/arXiv.2508.18083)
- Tinyanont, S., Wangnok, K., Andrews, J. E., et al. 2026, arXiv e-prints, arXiv:2602.02691, doi: [10.48550/arXiv.2602.02691](https://doi.org/10.48550/arXiv.2602.02691)
- Tody, D. 1986, in *Society of Photo-Optical Instrumentation Engineers (SPIE) Conference Series*, Vol. 627, *Instrumentation in astronomy VI*, ed. D. L. Crawford, 733, doi: [10.1117/12.968154](https://doi.org/10.1117/12.968154)
- Tody, D. 1993, in *Astronomical Society of the Pacific Conference Series*, Vol. 52, *Astronomical Data Analysis Software and Systems II*, ed. R. J. Hanisch, R. J. V. Brissenden, & J. Barnes, 173
- Tonry, J. L. 2011, *PASP*, 123, 58, doi: [10.1086/657997](https://doi.org/10.1086/657997)
- Tonry, J. L., Denneau, L., Heinze, A. N., et al. 2018, *PASP*, 130, 064505, doi: [10.1088/1538-3873/aabadf](https://doi.org/10.1088/1538-3873/aabadf)
- Troja, E., Piro, L., van Eerten, H., et al. 2017, *Nature*, 551, 71, doi: [10.1038/nature24290](https://doi.org/10.1038/nature24290)
- Utsumi, Y., Tanaka, M., Tominaga, N., et al. 2017, *PASJ*, 69, 101, doi: [10.1093/pasj/psx118](https://doi.org/10.1093/pasj/psx118)

- Valenti, S., Benetti, S., Cappellaro, E., et al. 2008, MNRAS, 383, 1485, doi: [10.1111/j.1365-2966.2007.12647.x](https://doi.org/10.1111/j.1365-2966.2007.12647.x)
- Valenti, S., Sand, D., Pastorello, A., et al. 2014, MNRAS, 438, 101, doi: [10.1093/mnrasl/slt171](https://doi.org/10.1093/mnrasl/slt171)
- Valenti, S., Howell, D. A., Stritzinger, M. D., et al. 2016, MNRAS, 459, 3939, doi: [10.1093/mnras/stw870](https://doi.org/10.1093/mnras/stw870)
- Valenti, S., Sand, D. J., Yang, S., et al. 2017, ApJL, 848, L24, doi: [10.3847/2041-8213/aa8edf](https://doi.org/10.3847/2041-8213/aa8edf)
- Ventura, P., Dell'Agli, F., Schneider, R., et al. 2014, MNRAS, 439, 977, doi: [10.1093/mnras/stu028](https://doi.org/10.1093/mnras/stu028)
- Virtanen, P., Gommers, R., Oliphant, T. E., et al. 2020, Nature Methods, 17, 261, doi: [10.1038/s41592-019-0686-2](https://doi.org/10.1038/s41592-019-0686-2)
- Wang, Y., Chen, C., & Zhang, B. 2026, Journal of High Energy Astrophysics, 50, 100490, doi: [10.1016/j.jheap.2025.100490](https://doi.org/10.1016/j.jheap.2025.100490)
- Woosley, S. E. 2019, ApJ, 878, 49, doi: [10.3847/1538-4357/ab1b41](https://doi.org/10.3847/1538-4357/ab1b41)
- Woosley, S. E., & Bloom, J. S. 2006, ARA&A, 44, 507, doi: [10.1146/annurev.astro.43.072103.15055810.48550/arXiv.astro-ph/0609142](https://doi.org/10.1146/annurev.astro.43.072103.15055810.48550/arXiv.astro-ph/0609142)
- Woosley, S. E., Heger, A., & Weaver, T. A. 2002, Reviews of Modern Physics, 74, 1015, doi: [10.1103/RevModPhys.74.1015](https://doi.org/10.1103/RevModPhys.74.1015)
- Yamanaka, M., Nagayama, T., Kumano, A., et al. 2026, arXiv e-prints, arXiv:2605.16916. <https://arxiv.org/abs/2605.16916>
- Yong, D., Kobayashi, C., Da Costa, G. S., et al. 2021, Nature, 595, 223, doi: [10.1038/s41586-021-03611-2](https://doi.org/10.1038/s41586-021-03611-2)